Hybrid Optical Fibers – An Innovative Platform for In-Fiber Photonic Devices

Markus Alexander Schmidt, Alexander Argyros, and Fabien Sorin*

The field of hybrid optical fibers is one of the most active research areas in current fiber optics and has the vision of integrating sophisticated materials inside fibers, which are not traditionally used in fiber optics. Novel in-fiber devices with unique properties have been developed, opening up new directions for fiber optics in fields of critical interest in modern research, such as biophotonics, environmental science, optoelectronics, metamaterials, remote sensing, medicine, or quantum optics. Here the recent progress in the field of hybrid optical fibers is reviewed from an application perspective, focusing on fiber-integrated devices enabled by including novel materials inside polymer and glass fibers. The topics discussed range from nanowire-based plasmonics and hyperlenses, to integrated semiconductor devices such as optoelectronic detectors, and intense light generation unlocked by highly nonlinear hybrid waveguides.

1. Introduction

Optical fibers have been an extremely successful platform for optical research and devices over the last 50 years. The strongest impact has been in optical networks and optical data communications, where fibers represent indispensable elements due to the ultralow loss window of silica fibers at near infrared wavelengths. Since the 1980s, optical fibers have become relevant in other areas of application including light generation using fiber lasers,[1,2] nonlinear optics,[3,4] medicine,[5–7] or remote and distributed strain- and temperature-sensing in environmental and infrastructure monitoring.[8,9] All the mentioned areas substantially benefit from the unique waveguiding properties of optical fibers, allowing the efficient and flexible transport of electromagnetic radiation via confined modes to desired locations.

Conventional optical fibers today consist for the most part of doped silica cores surrounded by pure silica claddings, and rely on total internal reflection at the core/cladding interface. A substantial extension of the functionality of optical fibers has been achieved in the 1990s by the discovery of photonic crystal fibers (PCFs).[10,11] These microstructured fibers include single or arrays of longitudinally invariant air holes of defined and various diameters, allowing the manipulation of the propagation of light inside the fibers in unique ways. Examples of such fibers, which are also referred to as microstructured optical fibers (MOFs), include hollow core photonic bandgap fibers[12–14] and endlessly single mode fibers, where the latter guides the light in a single optical mode for any combination of wavelength and core diameter.[15] All the mentioned fiber structures have now reached a technologically high level with the consequence that a large fraction of current MOF-related research focuses on the applications of MOFs rather than on new fiber geometries, which holds in particular for the field of solid-core fibers. One exception to this are recent developments in the area of silica hollow-core fibers, where anti-resonant fibers[16–19] or simplified hollow-core fibers[20–22] provide efficient light guidance in a hollow core with substantially reduced fabrication effort.

From the design perspective, however, fiber optics research has regained substantial interest during recent years by the integration of materials that are traditionally not used in fiber optics. This has opened up the entirely new research direction of hybrid optical fibers (HOFs) (**Figure 1**). This rapidly growing field is of interdisciplinary origin at the boundary between photonics, electrical engineering, materials science, optoelectronics, fiber optics, and chemistry. Particularly interesting are materials that are widely used in planar photonic devices that, if successfully integrated inside long, thin, and flexible fibers, could provide a novel class of one-dimensional photonic devices that are flexible and even potentially wearable. This actually defines the main idea of the field of hybrid optical fibers:

Prof. M. A. Schmidt
Leibniz Institute of Photonic Technology e.V.
Albert-Einstein-Str. 9, 07745 Jena, Germany
E-mail: markus.schmidt@ipht-jena.de
Prof. M. A. Schmidt
Otto Schott Institute of Material Research
Fraunhoferstr. 6, Friedrich-Schiller-University
07743 Jena, Germany
Prof. M. A. Schmidt
Abbe Center of Photonics, Friedrich-Schiller-University
Max-Wien-Platz 1, 07743 Jena, Germany
Prof. A. Argyros
Institute of Photonics and Optical Science (IPOS)
and School of Physics
A28 Physics Rd, The University of Sydney, NSW 2006, Australia
Prof. F. Sorin
Institute of Materials, Ecole Polytechnique Fédérale de Lausanne (EPFL)
Lausanne CH 1015, Switzerland

DOI: 10.1002/adom.201500319

implementing more and more functionalities into fibers to reach novel device functionalities, using an original substrate that has highly attractive mechanical and processing attributes compared to its planar counterparts. From the application perspective, the goal of HOF research comprises introducing new device-oriented functionalities into fibers to address highly relevant applications in fields such as photonics, energy harvesting, optoelectronics, biophotonics, or healthcare. One particularly important goal is to provide an alternative approach that can help, for instance, to remove the current bottleneck of mode-mismatch-induced losses at the planar device/fiber junctions. The inclusion of new materials into fibers has also extended fundamental research in fiber optics and opened up new frontiers in optics and photonics, as previously inaccessible areas such as plasmonics or metamaterials have been unlocked.

In this paper, we will review the efforts to include novel materials into various types of optical fibers mainly from an application-oriented perspective. We focus on photonics-related applications that go beyond optical transport to highlight the novel types of functionalities, or combination of multiple functionalities, that can be integrated over distributed length inside glass or polymer fibers. Other fiber-based devices more remote from the field of photonics, or looking at highly localized modification on the fiber tip for example, are discussed in other publications.[23–26] Rather than giving detailed insights into the various physical principles,[27,28] we present the different devices and their functionality with respect to the incorporated material, revealing the potential of the research field of hybrid optical fibers in general. As the entire field was triggered by disruptive improvements in fabrication technology, the review begins with a brief description of the three main fabrication techniques that involve the thermal drawing of a complete fiber device or a fiber template post-processing using deposition or filling, all allowing to incorporate "nontraditional" materials into fibers. Since the included materials define the functionalities of the resulting fibers, the main section of the review is split into three material parts. The first chapter of this section is dedicated to metallic wires in fibers, revealing promising applications within plasmonic sensing or in metamaterial-based super focusing. The next chapter targets semiconductors in fibers, showing the potential in, for instance, optoelectronic detection or energy saving and harvesting. The final chapter of the main section discusses new dielectric materials in fibers particularly focusing on novel nonlinear light-generation devices. The review closes with a discussion on future prospects of this promising and highly active field of fiber optics, highlighting areas where high-impact applications can be expected.

2. Fabrication Approaches

Substantial developments in fiber-drawing technology and the invention of new post-processing techniques have triggered strong advancements in the field of hybrid optical fibers during the past decade. As a result, the various fabrication approaches represent essential features in this research field and thus will be introduced here to give the reader a detailed overview of what is state-of-the-art in fabrication and, as a consequence, what materials could be included in optical fibers to date.

Markus A. Schmidt obtained a PhD from the University of Technology Hamburg-Harburg, Germany, 2005. From 2006 to 2012 he was a team leader in the division of Philip Russell at the Max Planck Institute for the Science of Light, Erlangen, Germany, and spent a research stay at Imperial College London, UK, 2011. Currently he is a professor at the Friedrich-Schiller University Jena and heads an independent research group at the Leibniz Institute of Photonic Technologies, Jena, Germany. His main interest targets combining optical fibers with photonic concepts within the areas of plasmonics, metamaterials and -surfaces, optofluidics, nonlinear optics, and bio- and nanophotonics.

Alexander Argyros completed a PhD in physics at the University of Sydney, Australia, 2006. He was a Research Fellow 2006–2008 at the Optical Fibre Technology Centre, University of Sydney. Since 2009 he has been at the School of Physics, University of Sydney, and an Associate Professor there since 2014. His interests include the interaction of electromagnetic radiation with wavelength and sub-wavelength scale structures in the context of optical fibres and other waveguides, photonic bandgap materials, metamaterials, and super-resolved imaging, across a broad spectrum from the visible to the terahertz.

Fabien Sorin obtained his PhD from the department of Materials Science at the Massachusetts Institute of Technology (MIT), Cambridge, USA. After 3 years at the Research Laboratory of Electronics, MIT, he joined Saint-Gobain and worked as a research scientist at the Saint-Gobain Research center in Aubervillers, France. In 2013, he joined the Ecole Polytechnique Fédérlae de Lausanne (EPFL, Switzerland) as an assistant professor in the Institute of Materials where he leads the Photonic Materials and Fiber devices laboratory. His research interests lie in investigating innovative materials, fabrication methods, and nanoscale device architectures to integrate advanced photonic and electronic functionalities within one-dimensional fibers and two-dimensional flexible and stretchable substrates.

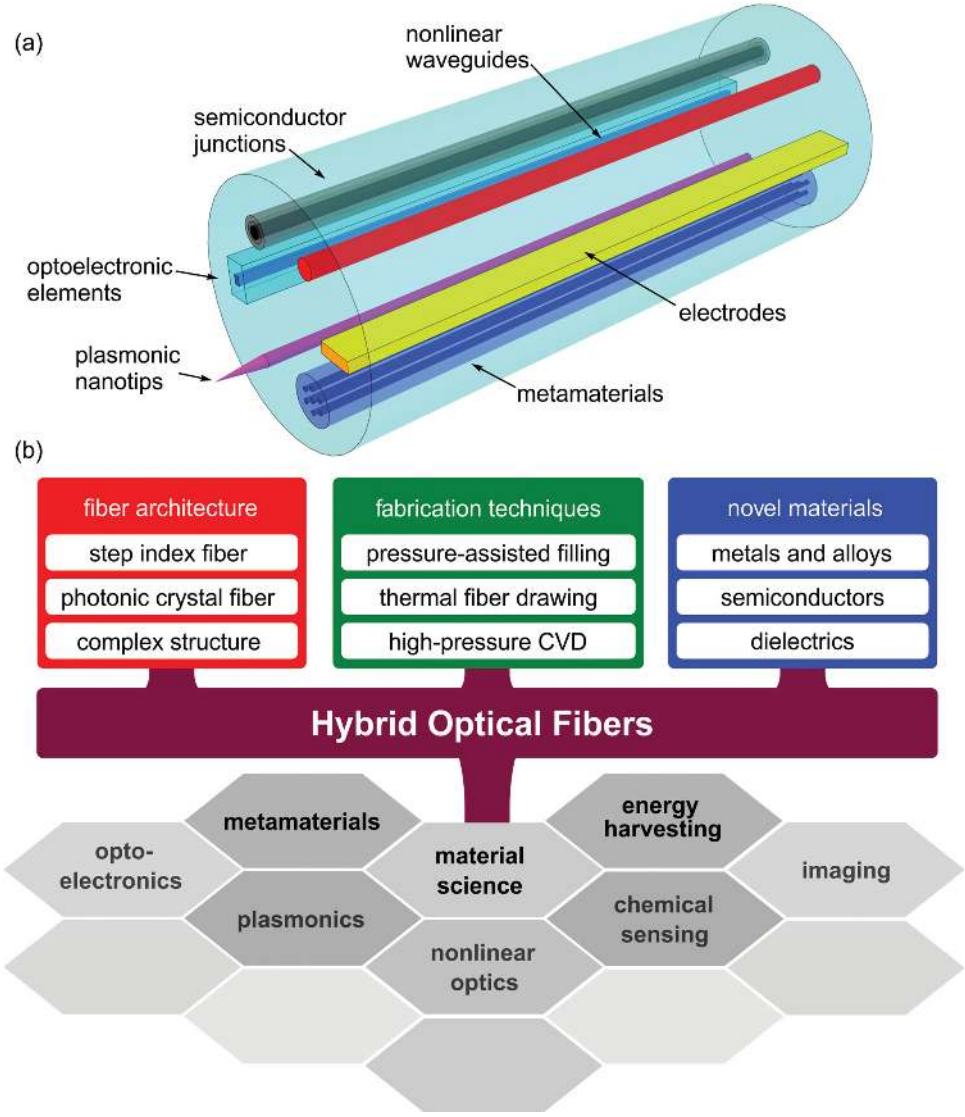

Figure 1. The concept of multimaterial hybrid fibers. a) Illustrative schematic showing the various functional elements and materials that can be integrated into fiber on the basis of the current fabrication technologies. b) Organigram of the concept, including the relevant fiber platforms, the various fabrication techniques, the involved materials and the areas in which hybrid optical fibers have become important.

2.1. Direct Thermal Drawing of Multimaterial Fibers

The first natural approach to integrate innovative functionalities inside optical fibers is to add novel materials at prescribed positions at the preform level, and to directly thermally draw the whole assembly into a long fiber. The principle of this approach mimics the way conventional silica telecommunication fibers are fabricated (a schematic of the process is shown in **Figure 2**a). This approach exhibits the main advantage of retaining the simplicity and scalability of the drawing process, which has several intrinsic attributes: 1) the fabrication of the preform is done at the macroscopic level and only requires simple and cost effective equipment that can precisely handle sub-millimeter feature sizes. The nanoscale structures inside the fiber, often required for efficient operation, are a result of the plastic deformation step that uniformly reduces the cross-section features along the entire fiber length. 2) Simultaneously, by the law of mass conservation, the act of scaling down results in the distribution of the volume into thin fibers, enabling the covering of macroscopic surfaces. It is not uncommon in the optical fiber industry to pull more than 1000 km of fiber that have an outer diameter of 125 µm. This corresponds to more than 125 m^2 of functional surface area, fabricated in a few hours of operation. 3) Fibers and ribbons are highly flexible and lightweight systems that are amenable to be integrated within surfaces, meshes, and fabrics. 4) Finally, this fabrication approach is also capable of simultaneously processing a variety of photonic and optoelectronic structures in a single processing step, as will be shown in this review.

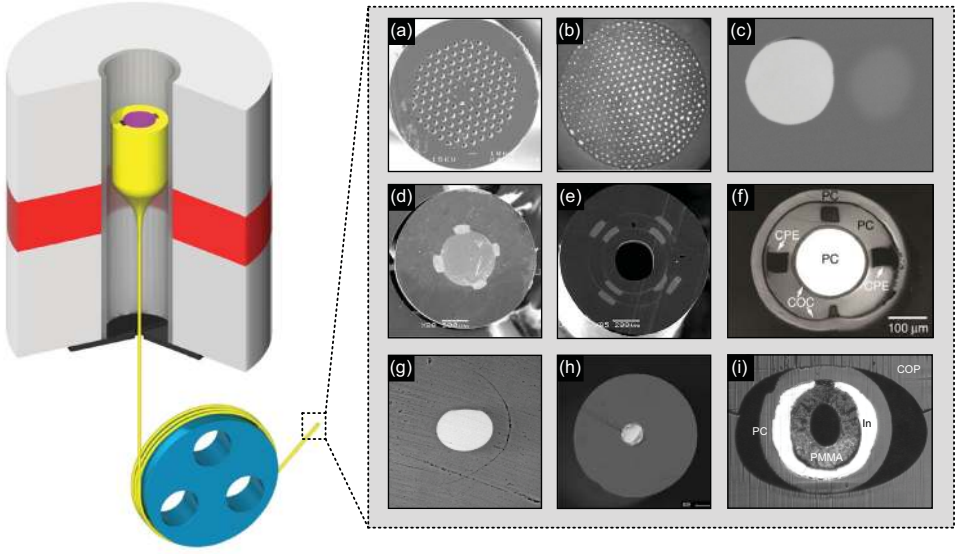

Figure 2. The direct thermal fiber-drawing technique. The left image schematically illustrates the operation principle of direct fiber drawing (acknowledgment to Dr. G. Lestoquoy and Prof. Y. Fink). The right figure shows examples of hybrid fibers which have been realized using fiber drawing: a) Copper wires inside PCF. Adapted with permission.[37] Copyright 2008, OSA. b) Array of indium microwires for THz application. Adapted with permission.[38] Copyright 2013, Macmillan Publishers Ltd. c) Gold nanowire inside modified step index fiber. Adapted.[39] Copyright 2010, OSA. d) Metal–insulator–semiconductor optoelectronic fiber. Adapted with permission.[40] Copyright 2004, Macmillan Publishers Ltd. e) Multijunction optoelectronic fiber. Adapted with permission.[41] Copyright 2009 American Chemical Society. f) Optical probe with a waveguiding structure, polymer composite electrodes and a microchannel. Adapted with permission.[42] g) Silicon-core optical fiber. Adapted with permission.[43] Copyright 2008, OSA. h) Phosphate glass-clad tellurium semiconductor core fibers. Reproduced with permission.[44] Copyright 2015, Elsevier. i) Polymer–metal magnetic resonator fiber. Adapted with permission.[45] Copyright 2001, OSA.

The first step in thermal drawing multimaterial HOFs (Figure 2a) is the fabrication of the macroscopic preform, which contains the complex structure as well as the relevant materials (or their precursors). Different materials are assembled in the preform via the thin-film rolling technique for cylindrical fibers,[25,29,30] via the stack-and-draw method commonly used for MOFs,[15,31] via extrusion,[24,32,33] or by machining and assembling materials together using consolidation in a vacuum oven or in a hot press.[25,34,35] The resulting preform assembly forms a solid object that represents the macroscopic version of the targeted fiber. It is thermally drawn into a fiber that maintains the cross sectional structure at the microscopic level along the entire fiber length, depending on the choice of the materials and the drawing parameters.

While the simplicity and scalability of the thermal drawing process is maintained with this approach, it sometimes requires thermal co-drawing of materials with different thermomechanical properties. In particular, photonic devices require at least two materials to exhibit an optical functionality, if only to create a refractive index contrast for optical guidance.[36] Given the creation of surface area during the drawing process, surface tension between materials will play a key role in the type of structures and geometries that can be achieved. To counteract this effect, viscosity engineering is typically conducted. In addition, crystallization, degradation, thermal expansion, chemical reaction and mixing have to be taken into account when designing a multimaterial fiber system. This imposes a set of requirements and hence a limited choice of material combinations which can be processed together inside the fibers. The main criteria for multimaterial drawing are as follows:

1) The cladding that makes most of the preform and holds the assembly together, must be processed at a relatively high viscosity, typically between 10^4 and 10^7 Pa s. This corresponds to a regime where the viscosity is low enough so that the material can be plastically deformed into fiber without breaking, while remaining high enough so that the mechanical integrity of the desired structure is maintained. With respect to this, glasses (e.g., silicates, phosphates, chalcogenides) and amorphous polymers represent ideal cladding candidates since they can be processed slightly above their glass transition temperature (T_g) and remain in a supercooled region with the right viscosity over extended range of temperature. This contrasts with crystalline materials where a first order phase transition from the solid to the liquid states induces an abrupt change of viscosity over a very narrow range of temperature that would be impossible to control in any practical systems.
2) An important requirement to consider for cladding materials in addition to the dependence of viscosity with temperature is the tendency to crystallize or degrade at high temperature. For glassy materials, a large supercooled region above their T_g is mandatory to avoid crystallization during the consolidation step as well as during drawing. As a consequence, the difference between the crystallization temperature and the glass transition temperature must be sufficiently large, typically more than 100 °C.
3) Crystalline materials can also be thermally drawn, but require processing at a drawing temperature that is higher than their melting point so that the material is in the liquid state during drawing. To maintain the desired cross-section

and avoid leakage, the crystalline material, that will flow as a liquid from the preform into the fiber, must be well encapsulated within a material that will flow at a high viscosity, within rigid (or higher viscosity) boundaries.

4) Another issue is heat diffusion between materials having different specific heats and thermal conductivities. As both viscosity and surface tension are material specific as well as temperature dependent, the temperature profile inside the preform is essential for drawing. Also, materials with high thermal conductivity such as metals will thermally shield other materials. This must be taken into account through careful positioning inside the preform or through modifying the materials that are shielded.
5) A large difference in thermal expansion coefficients must be avoided to eliminate excessive residual stresses in the resulting fibers.
6) The materials are brought together in a strongly confined space and at high temperature, which may result in diffusion of species and chemical reactions between the different compounds. These reactions are in many cases unwanted but sometimes desired and controlled. Enthalpy of formation and diffusion coefficients of species must be investigated before co-drawing materials.
7) Finally, the interplay between surface tension and viscosity imposes ultimate feature sizes of the different materials geometries (thin-films, hollow channels, etc.) targeted in the fiber, as will be discussed in the course of this review.

2.2. Pressure-Assisted Melt Filling

Another approach to implement hybrid fibers is to fabricate empty MOFs first and post-fill materials into the voids of the structures. One recently developed post-processing platform is pressure-assisted melt filling (PAMF).[46] Here, the material to-be-filled is liquefied via melting and pressed into the holes of the fiber matrix, which can be a MOF or just a capillary. In contrast to thermal drawing, this technique is comparably insensitive to a mismatch of thermal expansion coefficients or other highlighted requirements, and thus enables the introduction of a large variety of materials into fibers. It allows selectively infiltrating holes with various materials on lengths of the order of several tens of centimeters or more. Overall, this technology does not have the same strict compatibility criteria as co-drawing and instead includes only three prerequisites: 1) a low enough viscosity of the material to-be-introduced (<10 Pa s), 2) a filling temperature substantially below the softening point of the host glass, 3) no chemical reaction between host and filling material.[47,48] The last two constrains are most relaxed if silica fibers are used as hosts, allowing the use of materials with melting temperatures up to 1400 °C (viscosity of silica is 10^9 Pa s at that temperature).[49] Various experimental configuration of this technique have been implemented,[46,50] whereas the splice-filling setup represents the optimal compromise with respect to all experimental constrains (**Figure 3**a). This particular arrangement is straightforward to use, since it relies only on state-of-the-art splicing equipment and a simple furnace, which are available in almost any optics laboratory. Another key advantage of this particular configuration is the fact that only small initial material quantities of an almost arbitrary shape are required, making this approach especially valuable in cases where material availability is limited.

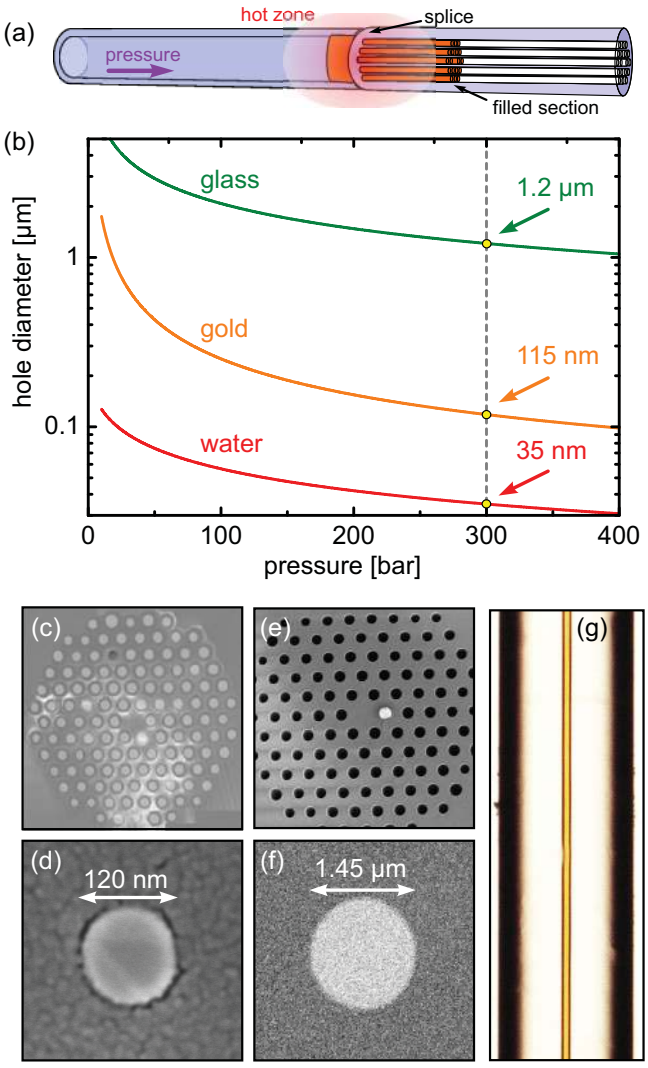

Figure 3. The pressure assisted melt filling technology. a) Scheme illustrating the filling procedure using a combination of splicing, heating and applying high gas pressure. b) Channel diameter that can be filled within 1 h to a 10 cm filling length as a function of pressure for three different materials. The grey dashed line exemplarily indicates 300 bars. Scanning electron micrograph (SEM) images of c) an array of metallic nanowires with central defect inside a silica fiber, and d) of the smallest gold nanowire fabricated so far using PAMF (diameter 120 nm, the end face is polished using focused ion-beam milling). Adapted with permission.[46] Copyright 2011, OSA. e) Germanium nanowire selectively filled into a hole in the first ring of a photonic crystal fiber. Adapted with permission.[58] Copyright 2008, OSA . f) Cross section of chalcogenide-silica step index fiber (core: $Ga_4Ge_{21}Sb_{10}S_{65}$, cladding: SiO_2). g) Microscopic side view of an As_2S_3 strand (diameter 4 µm) inside a silica capillary. Adapted with permission.[59] Copyright 2011, OSA.

The filling dynamics within PAMF are governed by the Lukas–Washburn equation, which describes the rheological properties of an incompressible liquid inside a cylindrical bore.[48,51] Neglecting gravitational forces (which is an excellent

approximation if external pressure is applied), the filling length L of a cylindrical capillary is given by

$$L = \frac{1}{2}\sqrt{(2R\gamma\cos(\theta) + R^2 p)t/\eta} \quad (1)$$

where p is the externally applied pressure, γ the surface tension of the liquid, θ the contact angle, R the hollow channel radius, η the dynamic viscosity and t the filling time. Real values of the filling length require the term in brackets to be larger than zero, leading to the definition of the minimum pressure $p_{min} = -(2\gamma/R)\cos\theta$ required to initiate the filling process. This equation reveals that with respect to PAMF, material can be categorized into two classes: In case $\theta > 90°$ (representing the case of metals and semiconductors), $p_{min} > 0$ and an external pressure is needed for filling. Since p_{min} is inversely proportional to the bore radius, smaller holes are generally more difficult to fill. Conversely, if $\theta < 90°$ (which typically holds for wetting liquids such as water or soft glasses), $p_{min} < 0$ and the liquid fills without the need of external pressure. It should be noted that even in the latter case, materials can have high viscosity at the filling temperature (such as glasses) and an external pressure is actually needed to keep the filling times reasonably short. The filling speed is mostly determined by the viscosity ($v \approx R/4(p/(\eta t))^{-0.5}$), which can vary over three orders of magnitude depending on the experimental situation and the material used. This fact is exemplified in Figure 3b, showing that the low viscosity of water and liquid gold allows filling nanometer size bores under typical experimental conditions, whereas the high viscosity of a typical glass restricts the minimum achievable diameters to the micrometer level.

It was experimentally shown that PAMF allows the filling of various types of materials into silica fiber: Filling noble metals allows the creation of longitudinal metallic nanowires (NWs) within fiber (Figure 3d), having led to the observation of kinds of plasmonic excitation such as spiraling surface plasmon polaritons (SPPs),[50,52] propagating plasmonic molecules[53] or hybridized plasmons (Figure 3c).[54] Nonlinear optical fiber waveguides with substantially improved optical properties have been established by incorporating chalcogenide glasses into silica fibers (Figure 3f,g), unlocking applications in coherent mid-IR supercontinuum generation,[55] frequency metrology[56] or in high-extinction optical filtering.[57] Furthermore, semiconductor wires have been selectively introduced into PCFs, showing distinct excitation of Mie-resonances and efficient in fiber polarization control (Figure 3e).[58]

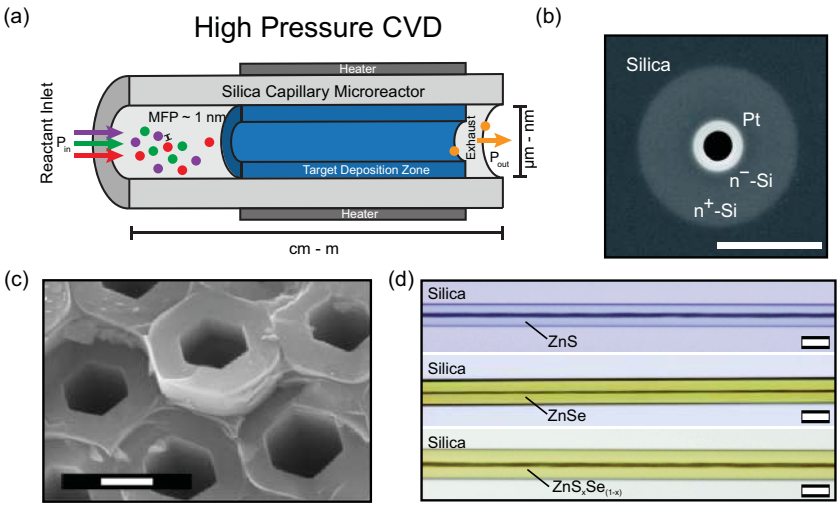

Figure 4. a) Sketch of the working principle of the high pressure chemical vapor deposition approach. b) Example of a concentric hybrid metal semiconductor junction integrated into a silica microstructured optical fiber. The structure represents a Pt/n-Si Schottky junction formed by sequential deposition of phosphorous doped n^+-Si, n^--Si and platinum layers. c) Hexagonal silicon tubes in a honeycomb MOF template (scale bar is 1 μm). d) Example of a recent work of in-fiber II–VI semiconductor wires (scale bar: 20 μm). Panels (a) and (d) adapted with permission.[67] Panel (b) reproduced with permission.[65] Copyright 2012, Macmillan Publishers Ltd. Panel (c) adapted with permission.[60] Copyright 2006, AAAS.

2.3. Modified Chemical Vapor Deposition

High-pressure chemical vapor deposition (HPCVD, **Figure 4**a) has turned out to be a versatile tool, especially for the integration of semiconductor materials into fibers. In this process, the holes of microstructured silica fibers act as chemical microreactors, in which the materials are deposited from the gas phase on the inner side walls.[60] The various gaseous ingredients needed for the process are inserted via high external pressure (of the order of several hundreds of bars), and the actual chemical reactions are either thermally stimulated or externally triggered via photoexcitation (e.g., by side focusing laser light onto the capillary).[61] The deposition process starts at the side walls of the bore, with the final film thickness being determined by the deposition time up to the point when the bore is completely filled. This technique was shown to be capable of producing semiconductor wires with diameters of the order of several micrometers down to hundreds of nanometers of various materials of extremely good optical and electrical quality.[60] By controlling the fabrication process and applying particular post-processing techniques,[62] the morphologies of the incorporated materials can be engineered, allowing the production of entirely amorphous,[63] polycrystalline[64] or even single-crystal semiconductor[61] wires inside MOFs. In addition to their optical functionalities, these structures allow the integration of semiconductor junctions directly into fibers, which makes them very attractive from the optoelectronic perspective.[65] The first experiments in the field of HPCVD were focused on doped and undoped single component semiconductor wires such as germanium[66] and silicon[64] (Figure 4c). One particularly interesting example is a concentric semiconductor multilayer of differently doped semiconductors in a PCF, which represented an entirely fiber-integrated semiconductor homojunction (Figure 4b).[65] More recent works extend towards integrating other semiconductor materials into microstructured fibers and capillaries such as II–VI semiconductors (e.g., ZnS or ZnSe)[67] (Figure 4d), which have promising application in light-generation schemes or optoelectronics.

3. Metallic Wires in Hybrid Fibers

From the traditional fiber optics perspective, integrating metals into optical fiber appears to be counter-productive, as the optical attenuation of metals is orders of magnitude larger than that of dielectrics, in particular than that of silica glass. However, the properties of providing negative dielectric functions and electrical conductivity enable the excitation of surface plasmon modes and the use of micro- and macroscopic electrical currents inside fibers, which represents a new degree of functionalities for fiber optics. A series of new fiber devices such as fiber-based plasmonic nanotips or hyperlenses have been established, which will be discussed below.

3.1. Metallic Wires for Simultaneous Optical Guidance and Electrical Transport

The first intuitive application one may think of when combining optical waveguides and electrical conductors is the simultaneous transport of light and electricity along a thin and flexible one dimensional system. A first fiber demonstrating such ability integrated a hollow core photonic bandgap structure surrounded by an array of metallic electrodes.[40] The fiber was characterized in terms of its modal attenuation and electrical wire resistivity along the fiber axis (**Figure 5**a). A particular area where such structures can have a profound impact is in various probes and endoscopic systems used in bioengineering, where optical excitation may trigger biological responses that can be recorded (or initiated) via an electrical signal. The thermal drawing process of multimaterial fibers turns out to be a unique way to realize flexible systems that could deliver and/or collect both optical and electrical signals. An important example of such class of devices is found in optogenetics, where neurons are modified to trigger reaction when exposed to light.[68] A HOF that integrates a waveguide, an array of metallic electrodes to collect electrical signal, and microchannels to deliver substances was recently proposed that could realize such functionality (Figure 5b).[69] The authors could demonstrate the recording of electrical signal from neurons in living rats thanks to these novel multimaterial fiber probes, paving the way towards the analysis of neural circuits in vivo. Other application areas in which in-fiber electrodes become highly relevant lie within superconductivity or in fast polarization switching or modulation, where particularly the former can open up new fields for fiber optics such as integrated single photon detection.[70–74]

It is important to highlight here that electrical conductivity has also been achieved by relying on other materials than crystalline solids. Polymer nanocomposites made out of a thermoplastic matrix loaded with carbon black particles have been shown to be compatible with the thermal drawing process in a variety of configurations.[35,75–77] While the conductivity remains orders of magnitude lower than for metals (around 1 S m^{-1} compared to 10^5–10^8 for metals), they can be processed at much higher viscosities, enabling complex shapes and architectures. It also enables a viscous boundary between elements that would otherwise react or mix with an interfacing liquid metal during the drawing process. Such composites were recently integrated

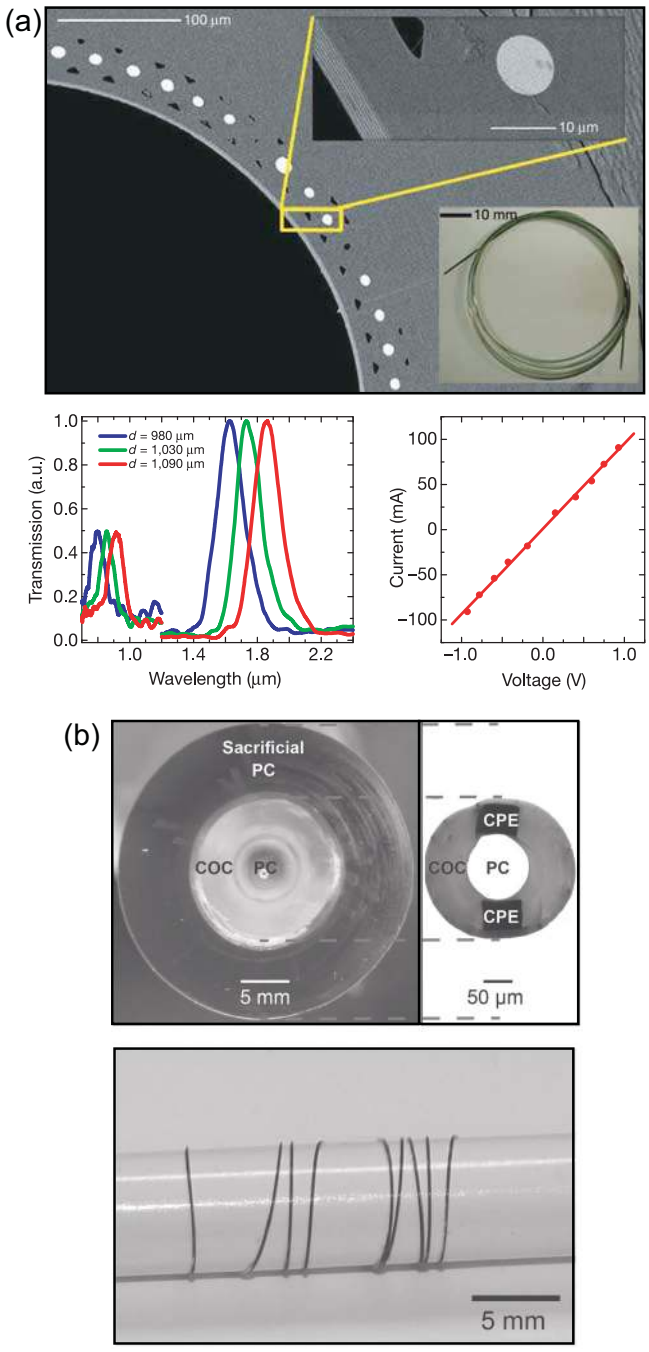

Figure 5. a) SEM micrograph of the cross-section of a hybrid fiber with 800 µm hollow core, omnidirectional mirror layers, metallic filament array and polymer cladding. Adapted with permission.[40] Copyright 2004, Macmillan Publishers Ltd. The inset shows eight pairs of quarter-wave As_2Se_3/PEI multilayers and one of the metallic filaments in the ring that is surrounding the mirror layers. A photograph of a 1-mm-thick, 1-m-long hybrid fiber is also shown. The graph below on the left shows the normalized transmission spectra of three different fibers, having diameters of 980, 1030 and 1090 µm. The graph to the right shows the measured electrical current along the 980 µm thick, 15 cm-long fiber as a function of applied bias voltage. b) Top: Optical micrographs of the all-polymer fiber probe with the PC core and COC cladding for index guiding, and the carbon black loaded polyethylene electrodes. Below is a picture of the fiber showing its flexibility and fine size. Adapted with permission.[42]

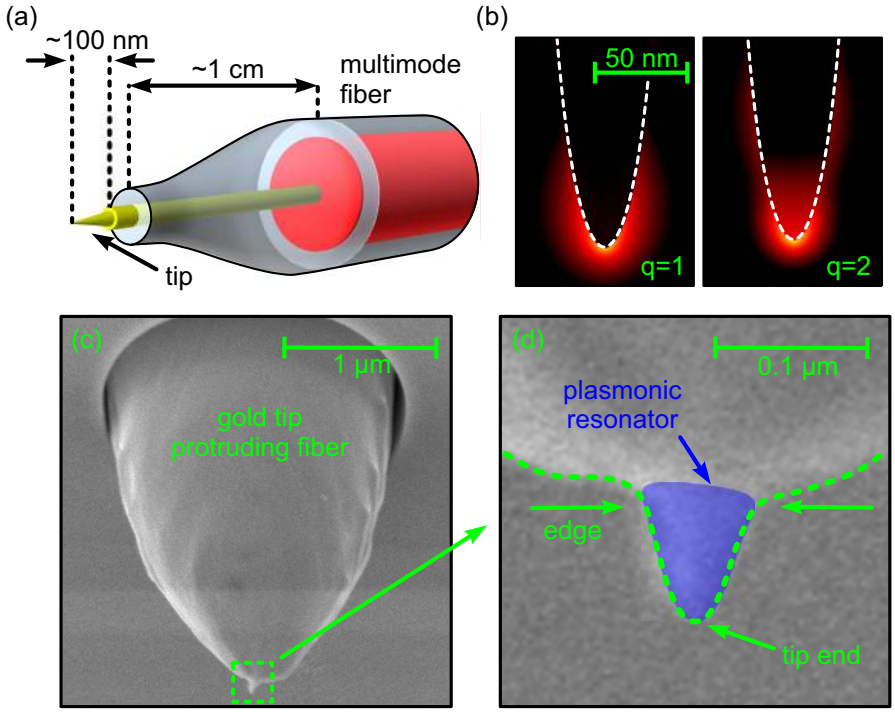

Figure 6. a) Schematic of the fiber-based near field nanoprobe (yellow: gold nanowire; red: core of multimode fiber). b) Simulations of the intensity distributions of the two lowest order plasmonic modes on the nanoprobe tip. The numbers indicate the plasmonic resonance order. c) Gold nanowire protruding from the end of the fiber probe. The dashed green square highlights the nanoscale plasmonic resonator at the wire's end. d) Close-up of the plasmonic resonator. The actual resonator is overlaid with a semi-transparent blue area for better visibility. The edge of the resonator is highlighted by the dashed green line. Reproduced with permission.[80] Copyright 2013, AIP Publishing LLC.

inside an all-polymer probe for the optical control and electrical response monitoring of the spinal cord and muscle function in vivo.[42] Figure 5b shows an optical micrograph of this structure highlighting the step-index guiding structure consisting of a polycarbonate (PC) core, a cylclo-olefin copolymer (COC) cladding, and two electrodes made from carbon-black loaded polyethylene (CPE). An alternative approach recently proposed for electrical conductivity inside optical fibers relies on ionic conductivity through the doping of a phosphate glass with silver.[78] The authors show a transparent glass that exhibits AC conductivity over a large range of frequencies, representing a way towards novel types of electronic and optical fiber devices.

3.2. Near-Field Probes Using Plasmonic Fibers

PAMF has been used by the Russell group in Erlangen and the Schmidt group in Jena to integrate metallic NWs into fiber, having enabled the observation of a new kind of plasmonic mode, the so-called spiraling surface plasmon polariton.[52,79] These special plasmonic modes formed the basis of a series of results within the area of plasmonics such as ultrastrong plasmonic hybridization[54] or the excitation of propagating plasmonic molecules.[53] Besides these rather fundamental studies, hybrid fibers including metallic NWs are also of relevance from the application point of view. One important example includes a novel kind of entirely fiber-integrated near-field plasmonic nanoprobe (**Figure 6**a).[80] The device consists of a tapered silica capillary incorporating a gold NW, attached to a standard multimode fiber. Using a sophisticated combination of wet-etching and cleaving, a nanoscale tip with dimensions significantly below 100 nm is formed, leading to a "tip-on-tip" structure (Figure 6c,d). The emergence of this tip can be explained by the ductility of the gold, which undergoes a plastic deformation when the NW-supporting capillary is cleaved. This subwavelength nanotip itself represents a small plasmonic resonator, supporting multiple localized surface plasmon resonances (LSPRs) in the visible spectral domain (two examples of scattering simulations approximating the tip by a metallic half-ellipsoid are shown in Figure 6b). The emergence of multiple LSPRs is rather exceptional and can be explained by a cavity model: here, the LSPR is formed by a fundamental SPP propagating to and from between the apex and the base of the ellipsoid. Two counter-propagating plasmons interfere, forming standing wave patterns, i.e. plasmon modes with defined mode orders.[80]

As a result of the nanoscale confinement, the LSPRs can be used to probe near fields with a resolution substantially below the operating wavelength (one example where the probe traces an evanescent field is shown in **Figure 7**a). Light scattered via the plasmon resonances partly scatters into the tapered capillary and is subsequently coupled into the multimode fiber, which ultimately guides the light to a desired location. The LSPRs strongly depend on the actual nanoscale shape of the tip, which makes it difficult to predict the exact spectral position of the resonance (the scattering spectra of three different tips and an example of the polarization dependence is shown in Figure 7b,c). This fact, which is a common issue to be considered in nanoscale photonics, remains uncritical for the tip presented, as the straightforward fabrication approach and the monolithic design have the potential for mass-production and fast characterization of individual nanotips.

3.3. Azimuthal Mode Polarization in Nanowire-Enhanced Fibers

Besides applications in plasmonics, fiber-integrated metallic NWs also allow for the creation of sophisticated polarization states with ultrahigh polarization discrimination. From the application point of view, beams with a cylindrical polarization state are interesting and are used in a large variety of

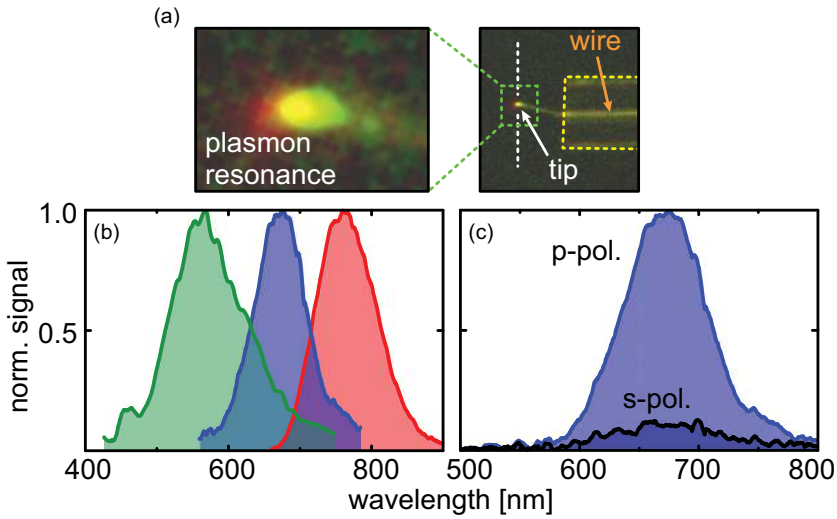

Figure 7. a) Microscope image of the scattered light of the plasmonic resonance when the nanoscale resonator is probing an evanescent field (right: end section of the nanoprobes (yellow dashed line: boundary of fiber; white dashed line: prism-air interface). Left: Close-up of the excited plasmonic resonance. b) Normalized scattering spectra of three different tips. d) Spectrum from one of the tips (corresponding to blue curve in (c)) for p- and s-polarized input light. Reproduced with permission.[80] Copyright 2013, AIP Publishing LLC.

always azimuthally polarized for a spectral interval spanning over an octave (600 nm < λ < 1.4 μm) with a polarization discrimination of more than 1:10^4. It is important to note that an entirely azimuthal polarization state can be converted straightforwardly to its radial counterpart simply via two wave plates. These unique polarization properties of this HOF device arise from the different fraction of magnetic field of the three supported modes inside the NW.[84] Since the fundamental and radially polarized modes have about one order of magnitude more field in the gold, only the azimuthal mode remains after a sufficient propagation distance (Figure 8b), leading to efficient azimuthal polarization. All three supported modes have annular shapes and rather equal excitation probabilities when being excited with an external Gaussian beam, giving rise to an overall azimuthal polarization efficiency of 10 dB, which is sufficient for many kinds of applications.

fields such as stimulated emission depletion microscopy[81] or superfocusing.[82]

A particularly important example of a HOF with unique polarization properties is a solid core PCF containing a gold NW in the center of the structure (**Figure 8**a and inset of b).[83] Regardless of input polarization state, it was shown that the output beam from a centimeter-long sample is

3.4. Hybrid Optical Fiber Metamaterials

In addition to single wires, arrays of metallic wires also allow the integration of novel functionalities into fiber. If the metallic features are substantially smaller than the operation wavelength, such an array becomes an effective medium, i.e., a metamaterial (MM), and its electromagnetic properties can be

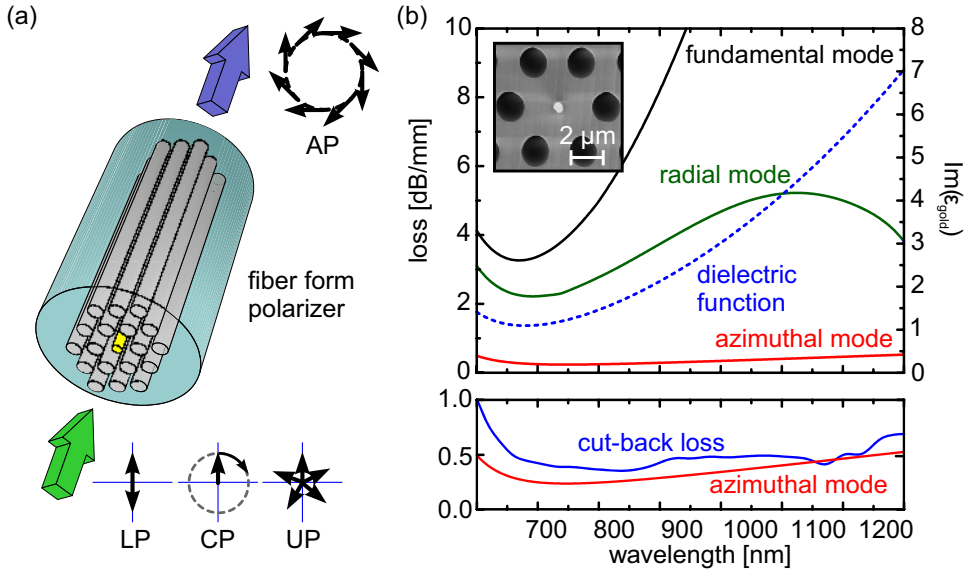

Figure 8. a) Operational principle and fiber geometry of the azimuthal mode polarizer (yellow: gold nanowire, light blue: silica, white: air holes). The green and blue arrows indicate the input and output light. The three lower sketches indicate linear (LP), circular (CP) and unpolarized (UP) light, and the upper sketch represents the azimuthal polarization state (AP). b) Simulated modal characteristics of the polarizer structure (Inset: SEM of the first ring of the polarizer). Upper panel: simulated attenuation spectra of the three important modes (dashed line refers to the imaginary part of the dielectric function of gold). Lower panel: experimental cut-back loss of the azimuthal mode compared with theory. Adapted with permission.[83] Copyright, IOP Publishing.

described by averaged or homogenized parameters which are controlled through the geometry of the structure.[85–87] Such wire-based MMs are classified as indefinite MM (iMM) with unique dispersion properties.[88] From a practical perspective, using direct drawing techniques for fabricating metamaterials[89] allows the production of large sample volumes required for real-world applications.

The experimental work demonstrating iMMs is based on using polymers as the dielectric (PMMA, polycarbonate, cyclo-olefin polymer (COP) Zeonex) and indium as the metal,[90] which satisfies the compatibility criteria for co-drawing described in Section 2.1 (melting point of indium is 157 °C, drawing temperature 200 °C). Fiber-based iMM were fabricated by a multiple version of the stack-and-draw process of single-wire fibers, leading to arrays of cm^2 areas containing more than 10^4 wires.[91,92] Such arrays behave as artificial metals for light polarized along the wires, with the incident electric field along the wires resulting in a current and a magnetic field that affects electrons in nearby wires. The result is a permittivity described by a Drude model with a geometry-dependent plasma frequency (**Figure 9**a).[88,93] The arrays thus behave as high-pass filters with a cut-on frequency that depends on the geometrical size of the structure.

Noncircular wires—a slotted cylinder resonator or split ring resonator—were also integrated into fiber by the direct drawing method to demonstrate a basic magnetic MM (Figure 9b).[45,94] A magnetic field perpendicular to the plane of the cylinder (parallel to the fiber) excites a current around the resonator resulting in both a magnetic field and an electric field across the gap of the resonator.[87] As such, it behaves as an LC circuit with a high frequency resonance that depends on the resonator's geometry, having a resonant permeability at high frequency.

The simplest application of these basic MM structures can be filters, particularly for the THz spectrum where components are still in relatively early development. One other possible application are hollow-core waveguides with extremely sub-wavelength cores, which rely on specific combinations of anisotropic positive and negative permeability in the cladding.[95,96]

3.5. Hybrid Fiber Hyperlens

A particular interesting application using iMMs are hyperlenses, capable of overcoming the diffraction limit to achieve super-resolved imaging and super-focusing.[38,97] The key property is the hyperbolic dispersion profile for extraordinary waves propagating along the array that occurs for these materials. This allows the propagation of high spatial frequency modes that would otherwise be evanescent, i.e., only present in the near field.[98,99] Their ability to propagate removes the diffraction limit, allowing the resolution of subwavelength features of an image at a large distance from the object.[38] From an optical fiber point of view, the wire array is analogous to a fiber bundle endoscope but with sub-wavelength pixels, or to a highly multimode fiber in which all modes are degenerate, thus any

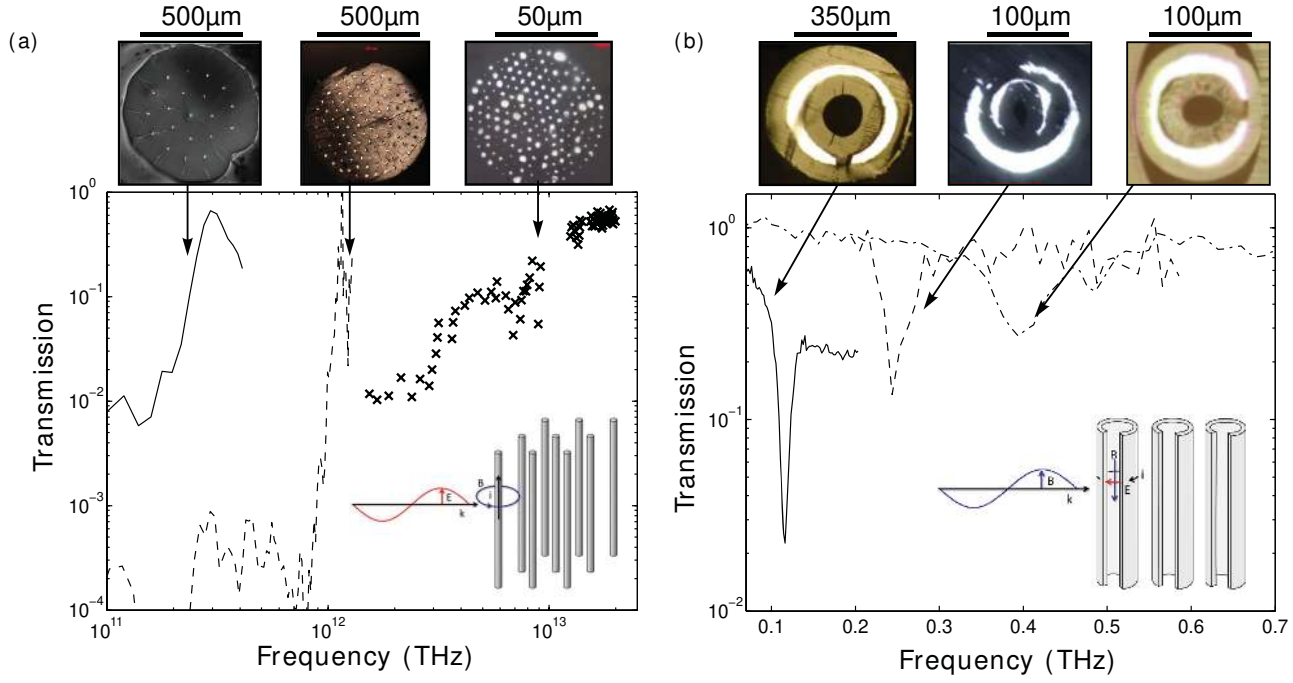

Figure 9. a) Transmission across various wire arrays. From left to right: 8 μm wires at 100 μm spacing results in cut-on frequencies of order 100 GHz, 12 μm wires at 50 μm spacing increases to 1 THz, and 2 μm wires at 7 μm scaling to 20 THz, spanning two orders of magnitude in frequency (inset shows the configuration). b) Transmission through various slotted cylinder resonator arrays. Propagation is perpendicular to the longitudinal axis of the resonators, with magnetic field parallel to the longitudinal axis (inset: polarization orientation relative to array). Left image of wire array adapted with permission.[91] Copyright 2010, AIP Publishing LLC. Central image of wire array adapted with permission.[92] Left and right resonator images adapted with permission.[45] Copyright 2011, OSA. Central image of resonator adapted with permission.[94] Copyright 2012, OSA.

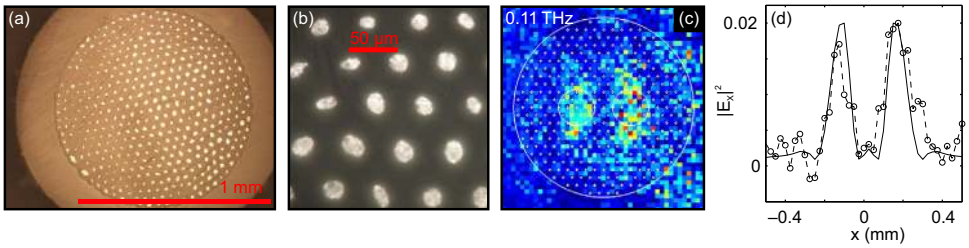

Figure 10. Metamaterial-based hyperlens using metallic wires in fiber. a) Optical microscope image of the structure containing 453 indium wires in a Zeonex background, with an external PMMA jacket. b) Close-up of the wires. c) Raw data from near field image at the end of a 3.4 mm hyperlens, with two 200 μm apertures with a 100 μm gap between them placed at the other end. d) Average power across the centre of the image in (c) (circles: data, solid line: calculations). Adapted with permission.[38] Copyright 2013, Macmillan Publishers Ltd.

excitation field is preserved along the propagation direction, including features of the near field.

Using direct drawing, a hyperlens consisting of 453 indium wires embedded in polymer was implemented, allowing super-resolved images in the THz domain.[38] The example presented here (**Figure 10**a,b) was able to resolve two 200 μm apertures separated by 100 μm at a wavelength of 2.7 mm, thus the smallest feature resolved corresponds to a dimension of $\lambda/27$.

In addition, a magnifying hyperlens consisting of a tapered wire array was demonstrated. Whilst extremely difficult to fabricate by other means, such a structure forms naturally in the fiber drawing process in the neck-down transition between the preform and fiber. The example in **Figure 11**a,b has an 8 mm diameter that tapers to a 1 mm diameter. Since there is no diffraction the taper allows super-focusing to subwavelength spot sizes, or the magnification of sub-wavelength features from below to above the diffraction limit with the result that such sub-wavelength features may be imaged by conventional optical components. The magnifying hyperlens presented here was able to super-focus a 1 mm spot to a minimum FWHM of $\lambda/28$ (Figure 11c,d).[38]

Finally, metallic domains may not only be used as high conductivity materials, but their optical properties can also be exploited to confine electromagnetic waves and hence provide a guiding mechanism for optical transport. Gold and copper wires surrounding a silica solid core have been used to make metallic optical fibers that rely on metallic confinement to guide light. Theoretical studies on these types of fibers also reveal the strong potential of metallic microwires and metamaterials to propose novel guiding mechanism and mode engineering for optical fibers.[50,54,96,100–102]

4. Semiconducting Materials in Hybrid Fibers

Semiconductors are key elements of any practically relevant optoelectronic system and are used in particular for the fast and efficient detection and modulation of electromagnetic radiation. One of the main motivations of the field of HOF is to integrate semiconductor functionalities directly into optical fibers, with the perspective of making a new generation of large area, flexible and even wearable photonic devices with efficiencies on par with or beyond their rigid planar counterparts. Various devices such as detectors or modulators have been implemented up to now and a selection of those will be discussed in this section.

4.1. Concentric Multimaterial Junction inside Silica Fibers

One important application of semiconductors in optoelectronics is the fast and efficient detection of light, in particular NIR wavelengths that form the basis of telecommunications. Many of the currently used integrated detector schemes are based on planar devices, which have the intrinsic drawback of imposing

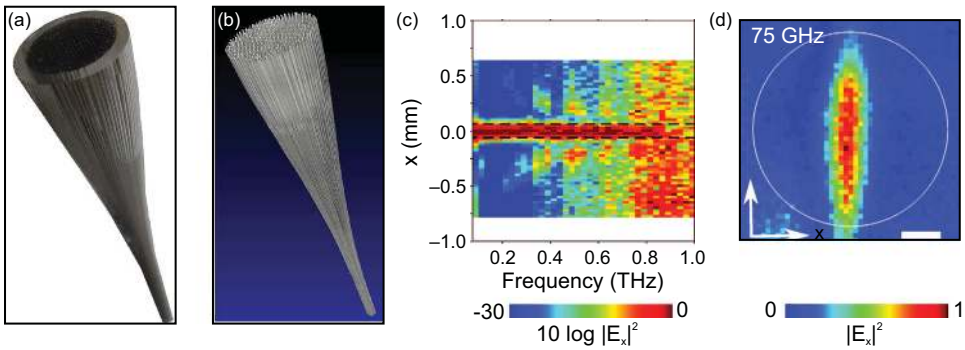

Figure 11. a) Photograph and b) computer-tomography-scan of the tapered hyperlens. A 1 mm diameter aperture was placed at the large end of the taper and illuminated, and near field images were taken at the narrow end of the taper. c) The width (along x) of the resulting super-focused image at the narrow end of the taper as a function of frequency. d) An example image at the specified frequency, showing focusing to a FWHM of $\lambda/28$ in the x-direction. The spread in the y-direction arises from the ordinary waves diffracting. Adapted with permission.[38] Copyright 2013, Macmillan Publishers Ltd.

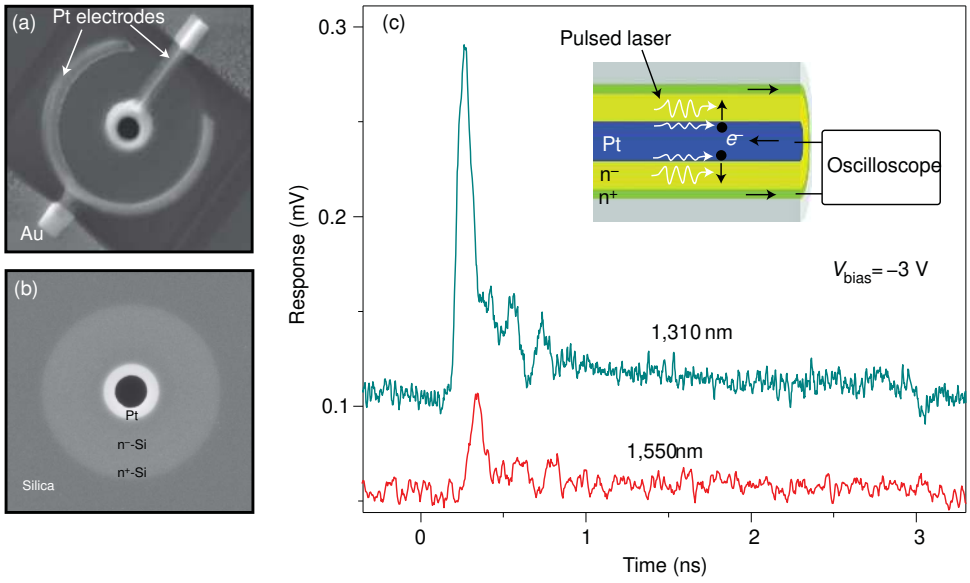

Figure 12. Optoelectronic concentric semiconductor junction integrated into a photonic crystal fiber. a) SEM image of the relevant section, which represents a Pt/n-Si Schottky junction formed by sequential deposition of phosphorous doped n^+-Si, n^--Si and platinum layers. b) Electrodes fabricated on the Pt/n-Si diode using focused-ion-beam-milling, with platinum electrodes contacting the platinum and n^+-Si layers. c) Photodetection response to 10 ps laser pulses (two curves refer to two different excitation wavelength (blue: 1.31 μm, red: 1.55 μm). There is an intentional d.c. offset of the two response curves for clarity.) Inset: internal photoemission process, carrier transport and collection scheme. Adapted with permission.[65] Copyright 2012, Macmillan Publishers Ltd.

inevitable loss at the fiber/planar device junction. The optimal solution to this problem is to include the detector functionality directly into the fibers. One particular interesting approach was presented by the Badding group,[65] where they used HPCVD to deposit multilayers of differently doped crystalline semiconductor materials inside silica capillaries and in selected holes of PCFs (**Figure 12**a). It was shown that a concentric multilayer consisting of a n^+/n^-/Pt junction in a 15 μm diameter hole supported a fundamental HE_{11} waveguide mode with about 30 dB/mm at telecommunication wavelengths (Figure 12b). Using a sophisticated contacting scheme this device showed rise and fall times of the order of several tens of picoseconds when excited by picosecond optical pulses (Figure 12c), which is a sufficient figure for many optoelectronic detection applications.

In a next step a junction with reduced complexity was created inside a selected hole of a PCF, where strong coupling between the fundamental PCF mode and the modes in the junction was observed. This example of an integrated optoelectronic semiconductor junction clearly emphasizes the potential of the vision of all-in-fiber detection, which can change or even revolutionize the field of optoelectronics.

4.2. Thermally Drawn Optoelectronic Fibers

While semiconductor devices with excellent performance can be achieved using HPCVD techniques, the main limitation of such an approach is its scalability, as only short fiber lengths can be functionalized. Integrating semiconducting functionalities, traditionally reserved for smaller scale and rigid wafer substrates, inside flexible 1D systems with the length and surface associated with optical fibers, can herald a novel path towards large area, flexible, and even wearable optoelectronic devices. Several applications can be envisioned and have been proposed for these one dimensional fiber systems (as opposed to point devices) in imaging,[41,103,104] industrial monitoring,[105] remote and distributed sensing,[34,35] energy harvesting[75,106] and functional fabrics.[25,41,107] A promising strategy to realize this vision is to employ the multimaterial thermal drawing approach to directly integrate semiconducting materials in contact with metals and insulators in prescribed architectures. While we have seen so far that polymers and glasses can be co-drawn with metallic wires, a photoconductive element must be found that is compatible with the thermal drawing process. Chalcogenide glasses, a class of materials based on the Chalcogen elements (S, Se, Te), have the double advantage of being compatible with this process, and exhibiting relevant optoelectronic properties that are tunable depending on their composition (with As, Ge or Sn being typical additive materials). They have been extensively used in photonic crystal fibers owing to their large refractive index[29,30] and strongly nonlinear properties.[24,32,108,109] They are also used for IR fibers and in particular Multimaterial IR fibers, as pure chalcogenide glasses can exhibit extremely low absorption in different parts of the IR spectrum depending on their composition.[109,110] In the visible, however, chalcogenides can be highly absorbing and materials such as Selenium can exhibit high charge (hole) mobilities in its crystalline hexagonal phase. Se also exhibtis a high photoconductivity[111,112] and is extensively used in xerography plates, rectifying junctions as well as thin-film photovoltaics.[111,113–118] Chalcogenide glasses hence constitute ideal candidates to fabricate optoelectronic one-dimensional flexible systems fabricated via the thermal drawing technique. In **Figure 13**a, we show a picture of a preform-to-fiber assembly where metallic electrodes

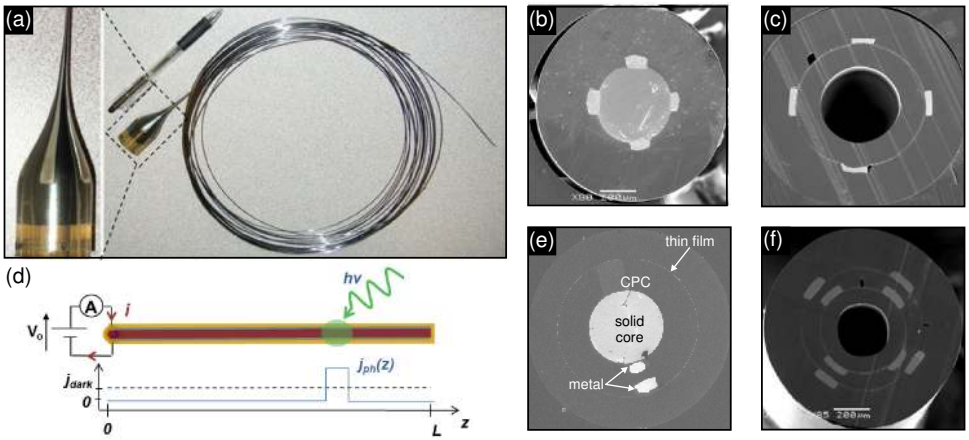

Figure 13. a) Preform pulled into extended fiber including metallic electrodes seen as the grey rectangles in the picture. The electrodes interface with a Selenium-based chalcogenide glass layer (black part). Adapted with permission.[34] b) SEM cross section of a solid core fiber contacted by four metallic electrodes. Adapted with permission.[40] Copyright 2004, Macmillan Publishers Ltd. c) SEM cross-section of an optoelectronic fiber with a thin chalcogenide glass layer contacted by four metallic electrodes. Adapted with permission.[34] d) Schematic of light detection in one-dimensional photodetecting fibers. e) SEM cross-section of a fiber capable of localizing optical beams. CPC electrodes contacting both a thin film and a solid core glass domains inducing a non-axially symmetric drop of potential between the CPC and metallic electrodes. Adapted with permission.[76] Copyright 2010, OSA. f) SEM cross-section of a dual-ring optoelectronic fiber: two thin chalcogenide glass layers are vertically integrated and each connected by four metallic electrodes. Adapted with permission.[41] Copyright 2009, American Chemical Society.

are in contact with an appearing black layer made out of a Selenium-based chalcaogenide glass.

4.2.1. Amorphous Semiconductor-based Optoelectronic Fibers

The first metal-insulator-semiconductor optoelectronic fibers were demonstrated in 2004, where a chalcogenide glass core contacted by four metallic electrodes and surrounded by a transparent polymer cladding showed photodetecting capabilities (Figure 13b).[40] Further optical functionality was integrated when a Fabry–Perot cavity was added around the photodetecting structure to select the operating wavelength. Solid-core optoelectronic fibers were also shown to be sensitive to thermal radiation,[107] and to exhibit a great potential for large area interacting screens, meshes and fabrics. In particular, a lensless imaging system was demonstrated using two grids made out of such solid-core optoelectronic fibers.[103]

A deeper investigation of the basic structure–property relations in these novel form factor devices has revealed a path towards the transition to sub-wavelength semiconducting thin-film architectures in subsequent studies.[34] By removing the core material, a drastic reduction of the dark current and hence the associated electrical noise could be achieved without reducing the device's responsivity. In addition to an improved sensitivity, the integration of thin-film configurations has paved the way towards complex in-fiber architectures, which exhibit advanced and unforeseen functionalities. For example, a thermal sensing layer could be added around Bragg mirror of a photonic bandgap fibers. The resulting fiber had the ability to monitor itself against the presence of defects that could locally heat and destroy the polymer cladding.[107] One could also in principle integrate an arbitrary number of thin semiconducting layers within a single fiber, enabling increasingly advanced functioanlities. For example, by cascading several of such layers in a single fiber, each independently electrically contacted by metallic electrodes (Figure 13f), fibers that could sense not only impinging optical wave fronts but also extract their angle of incidence, wavelength and power were fabricated. Assembling such photodetecting fibers into a flexible grid, the Fink group at MIT could demonstrate a fiber-based fabric capable of generating optical images.[41,104]

This first generation of optoelectronic fibers has given rise to new 1D devices that can be integrated in myriad of applications and configurations. The examples presented so far still suffer, however, from three main limitations: 1) the axial symmetry that prevents the extraction of information on the stimuli distribution along the fiber axis; 2) the amorphous nature of the semiconducting material that result in rather poor optoelectronic properties, and; 3) the limited available semiconducting materials. To address the first point, a configuration was proposed to localize axial position of one or more incident beams impinging onto a photodetecting fiber (Figure 13d).[76] A fiber that integrates a semiconducting thin film, a solid core and a carbon black loaded polycarbonate (CPC) resistor could localize a beam with a 1 cm resolution over a 1 meter long fiber. The low conductivity of the CPC material compared to its metallic electrode counterpart enabled the tailoring of the electric field distribution along the fiber axis. By measuring the current generated while varying the potential drop applied at both fiber ends, one can measure independent currents and hence reconstruct the location of the beam.

4.2.2. Crystalline Semiconductor-based Optoelectronic Fibers

While these geometrical improvements have enabled the increase of the performance and flexibility of complex fiber devices, the materials and their phases need to be revisited to

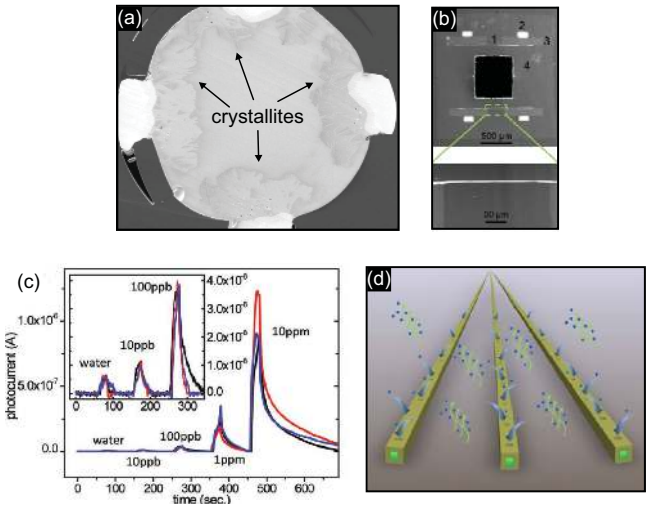

Figure 14. a) SEM micrograph of a solid chalcogenide glass core ($As_{52}Se_{40}Te_8$) fiber after a post-drawing thermal annealing treatment that exhibits crystal growth nucleating for the most part from the interfacing crystalline electrodes. Adapted with permission.[119] b) SEM cross-section of a square shape semiconducting Multimaterial fiber having a hollow core surrounded by two thin $Se_{97}S_3$ layers (1), connected by CPC (3) and metallic electrodes (2), all embedded in a polymer cladding (4). c) Photoresponse of the fiber shown in (b). The inner walls were coated with a chemoluminescent layer that responds to triacetone triperoxide (TATP) molecules. When TATP molecules flow inside the hollow core, they attach to the CL layer and a fluorescent signal is admitted and intercepted by the Se-based photodetecting devices. The increase of photocurrent as the molecules flow over time is shown in the graph.[35] d) Schematic of the fiber distributed sensor concept with novel multimaterial fibers interacting with the world in novel ways. Adapted with permission.[35]

improve light-sensing fibers further. Indeed, thermally drawn fibers with amorphous materials reveal the relatively poor electronic and optoelectronic properties due to the glassy state of the semiconductors. To alleviate this limitation, two approaches have been proposed:

1) Crystalline semiconductor phases inside the fiber can be established when subjected to a specific post-drawing heat treatment.[119,120] One example includes crystallites that have grown from the tin electrodes interfacing with a chalcogenide glass ($As_{52}Se_{40}Te_8$) after a post-drawing annealing treatment (**Figure 14**a).[119] This was shown to drastically reduce the resistivity of the glass and enabled a novel electronic system to be realized. The in-fiber post-drawing crystallization of a selenium layer was also demonstrated (Figure 14b), which highlighted the level of sensitivity that can be achieved by optoelectronic fibers. The photodetecting sensor exhibited a noise equivalent power of below 1 nW/√Hz.[35] This sensor was used in a novel configuration to detect chemicals thanks to a chemoluminescent (CL) coating that changes its optical emission upon exposure to the targeted substance. Instead of using purely optical fiber to collect the CL signal and guide it to distal detectors,[121] a multimaterial hybrid fiber with a semiconducting thin-film-based photodetector embedded in the fiber itself and distributed along the entire fiber length was implemented (Figure 14b). This configuration alleviates the optical losses experienced by the CL signal in purely optical systems. Indeed, most of the emitted photons are directly absorbed and converted into an electrical signal by the surrounding semiconducting layer at the spot where the hazardous chemical triggered the emission. The sensitivity of this fiber sensor is hence no longer dictated by a signal collection deficiency, but is governed by the performance of the distributed photodetector. This approach was demonstrated to exhibit performance on par with state-of-the-art systems, with a sensitivity of a few tens of parts per billion (Figure 14c). This highlights the strong potential for distal and distributed sensing of a variety of stimuli enabled by the multimaterial fiber approach (schematically depicted in Figure 14d).[35]
2) Rather than using re-crystallization, the second approach relies on directly drawing crystalline semiconducting material as a melt. This approach has the advantage of accessing a wider class of materials, as long as a compatible glassy cladding can be found to encapsulate the liquid as it flows from preform to fiber. In particular, materials more commonly used in electronic and optoelectronic components such as silicon and germanium can be integrated with this technique, which can bring a higher level of performance, novel optoelectronic applications and superior optical properties. So far, it is the particular optical properties of crystalline semiconductors, rather than their optoelectronic attributes, that has been exploited in crystalline core optical fibers. Si and Ge for example are highly nonlinear materials with Raman gain coefficients much higher than silica and are transparent in the IR (examples of Si core fiber shown in Figure 2g).[122,123] The first attempt to integrate a Si core in a silica cladding was done in 2008 by introducing a Si rod inside a silica tube.[43] The melting point of Si is at around 1416 °C, well below the typical drawing temperature of silica around 2000 °C. Note that the approach of introducing Silicon powder into a tube under vacuum has also been proposed.[124] Other materials have been drawn with a similar approach such as Ge, InSb, or even sapphire derived all-glass optical fibers.[125–127] At such high temperature, effects such as diffusion, chemical reactions and the formation of grain boundaries upon cooling and solidification can be expected. This was recently highlighted in work where an aluminium rod inside a silica cladding at the preform level resulted in a Silicon core and alumina domains in the fiber.[128] Extensive work has also been performed to elucidate and control nucleation and grain growth, in order to extend the length of single crystal domains along the fiber axis.[129–131] Note also that Se and Te cores have recently been co-drawn inside phosphate glasses, which paves the way towards integrating semiconducting materials at a novel temperature range.[44,132] To realize optoelectronic fibers with these materials, however, the difficulty remains of finding compatible materials to act as electrodes that do not mix or react with the molten semiconductor during drawing.

4.2.3. Synthesis of Novel Compounds during Thermal Drawing

Another intriguing phenomenon recently shown in multimaterial HOFs is the compound formation induced by the drawing process.[106,128,133] During thermal drawing, materials

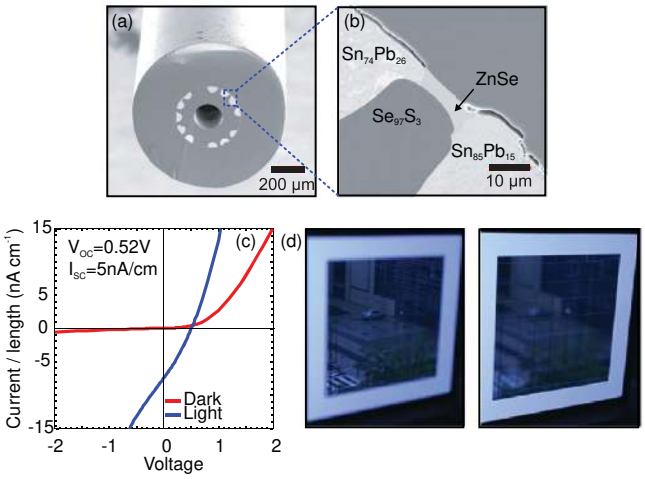

Figure 15. a) SEM micrograph of a photodiode fiber, with a zoom-in on the co-planar structure showing the two electrodes (eutectics SnPb and SnZn) and the heterojunction between a Se-based layer and a ZnSe domain that formed during the drawing process. b) *I–V* curve in the dark and under illumination, revealing an open-circuit voltage of 0.52 V. c) Example of a sparse fiber mesh covering a window that could seamlessly act as an air or temperature monitoring unit, or harness energy from the environment. Adapted with permission.[106] Copyright 2011, National Academy of Sciences.

are brought together at high temperature and confined in a small cross-sectional architecture. Depending on the materials in contact, the interdiffusion coefficients and the enthalpy of formation of various compounds, it can be anticipated that synthesis may occur and different materials end up in the fiber compared to those found in the preform. The first work that presented what could be named a multimaterial fiber draw synthesis approach was realized after the volatization of some elements initially in the core of the preform, resulting in a different composition in the fiber.[134]

The only functional optoelectronic device using fiber draw synthesis was recently presented where a $Se_{97}S_3$ layer was brought in contact with a $Sn_{85}Zn_{15}$ eutectic electrode.[106] It is argued in this study, and was investigated further later in a subsequent study by the same group,[133] that ZnSe compound was formed after diffusion of the Zn from the electrode and reaction with Se. This layer with a large bandgap in between the Se layer and the metal (**Figure 15**a), would explain the formation of a heterojunction that induced a barrier to the transport of holes. The junction realized in the fiber exhibited a built-in voltage of around 0.5 V (Figure 15b). While the short circuit current was very small given the unoptimized parallel configuration in the fiber, the high open circuit voltage opens the way towards creating truly distributed and scalable photovoltaic fibers that could combine the flexibility of polymers with the efficiency of inorganic compounds.

It should be noted that this approach contrasts with other commonly used ways to integrate photovoltaic functionalities into fiber using HPCVD or solution process layers onto existing fibers.[135,136] Another recently proposed approach is to use the multimaterial fiber platform for energy harvesting, which relies on the integration of a dye inside a polymer fiber that was shaped to focus the incoming light from the sun onto the dye material. The re-emitted light is then guided to the fiber extremities where solar cells are positioned, effectively using the fiber as large area concentrators.[137]

5. Novel Dielectric Materials in Fibers

By choosing the dielectric properties of the material to be integrated into the fibers, the characteristics of the propagating waveguide modes can be engineered almost as desired. This degree of freedom is of interest for many applications and in particular for light generation schemes relying on ultrafast nonlinear optical effect, as pulse dispersions can be adjusted in a way beyond those of standard all-silica fibers. Dispersion engineering is extremely relevant, for example, broadband supercontinuum generation, as shown by the examples discussed below. Moreover, the integration of sophisticated dielectrics into fiber leads to novel and improved functionalities, examples of which include strong Faraday rotation or broadband in-fiber polarization.

5.1. Nonlinear Light Generation

The efficient and broadband generation of light is clearly an important prerequisite for any practically relevant photonic system. Nonlinear optics and in particular super-continuum generation (SCG) using optical fibers represents a promising path to achieving this goal, as the optical Kerr effect together with a strong modal confinement can enable efficient octave-spanning spectral broadening via a combination of various nonlinear effects (a detailed review of the field of fiber-based SCG can be found in the literature.[138,139] Accessing new spectral domains such as the mid-IR requires using novel materials such as chalcogenide[140–142] or semiconductors,[143,144] which ought to combine strong modal confinement, engineered modal dispersion, efficient launching and light extraction and high optical nonlinearity. HOFs hold a great potential in this field, as they naturally address all these mentioned issues on an entirely integrated waveguide platform.

One example of such a light-generating hybrid waveguide is a chalcogenide-silica fiber,[59] being composed of a cylindrical chalcogenide core and a silica matrix (**Figure 16**a).[55,56,145] As we highlighted above, amorphous chalcogenide glasses are particularly interesting due to their intrinsic high refractive index (>2 for visible and infrared wavelengths), their extended transparency windows (≈0.6 μm < λ < 10 μm) and their strong nonlinear response (the nonlinear coefficient of chalcogenides is about two orders of magnitude larger than that of silica glass).[146] Using PAMF centimeter-long continuous chalcogenide strands with predefined diameters of the order of several micrometers have been integrated into silica capillaries.[56,145,147] Since the silica remains chemically inert during filling, the filled-in As_2S_3 reveals bulk optical properties, which is favorable from the simulation as well as from the experimental perspective. This is especially important with respect to SCG, which requires precise adjustment of the group velocity dispersion to minimize frequency walk-off. Incoupling efficiency has been boosted via the integration of a down-taper (so-called photonic nanospike)

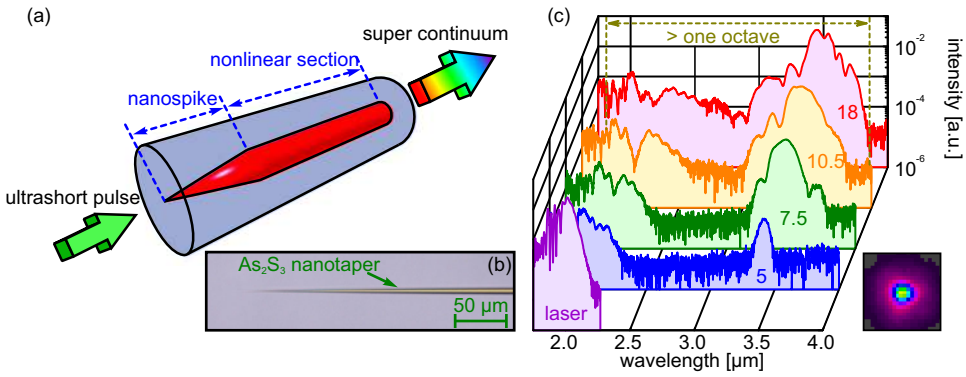

Figure 16. Coherent mid-IR supercontinuum generation using a chalcogenide nanospike. a) Schematic of the chalcogenide nanospike embedded in silica (red: chalcogenide; blue: silica). b) Side-view of the nanospike section. c) Supercontinuum spectra taken at different pulse energies when ultrashort pulses are coupled into the waveguide via the nanospike (12% coupling efficiency, blue: 5.0 pJ, green: 7.5 pJ, orange: 10.5 pJ, red: 18 pJ, pulse length 60 fs). The purple curve represents the laser spectrum. The lower right image shows the measured near-field profile of the mode at the output end of the waveguide. Adapted with permission.[55] Copyright 2013, OSA.

into the front part of the hybrid fiber (Figure 16b), which allows to locally match the external beam to the mode inside the spike.[55] The coupled energy is then adiabatically transferred into the chalcogenide core, leading to an increase in coupling efficiency by a factor of 60 into the deep subwavelength, 1 µm wide chalcogenide core (excitation wavelength: 1.9 µm). The increasing modal attenuation of that device is entirely dominated by the silica cladding and not by the chalcogenide core for $\lambda > 2$ µm, reaching 1 dB mm^{-1} at 4 µm which defines a natural boundary for SCG in this structure.

Exciting the fundamental mode in a 2 mm long sample using an intense femtosecond laser pulse (center wavelength: 1.9 µm, pulse width: 65 fs) leads to octave-spanning SCG up to a wavelength of 3.9 µm at a pulse energy of only 18 pJ (Figure 16c). The chalcogenide–silica hybrid fiber thus represents a new kind of fiber-based light source for the mid-IR, a highly relevant spectral domain that demands intense and coherent sources for spectroscopic or analytic applications. Recent simulations and experiments reveal that the generated spectra are coherent over the entire generated bandwidth,[56] which makes this hybrid device interesting for frequency comb-based metrology in a spectral domain beyond all-silica fibers. Furthermore, double nanospike chalcogenide-silica fibers have been recently implemented showing substantially improved outcoupling efficiencies.[145]

Besides PAMF, highly nonlinear materials can also be incorporated into microstructured fibers via direct fiber drawing, examples of which include SCG inside chalcogenide wires embedded in polymer matrices. The Abouraddy group at Creol showed that dual layer chalcogenide nanotapers can be integrated into a thermoplastic polymer jacket (**Figure 17**a).[148] The dispersion engineering has been achieved via tapering the structure down to a remaining chalcogenide core diameter of only 500 nm over a length of 50 mm, allowing the generation of broadband light over an octave-spanning spectral bandwidth when pumped with femtosecond pulses (center pulse wavelength: 1.55 µm, pulse energies ≈ 40 pJ).

In another recent work strong modulation instability in the mid-IR spectral domain was observed when a hybrid polymer–chalcogenide optical microwire was pumped with a femtosecond optical parametric oscillator operating at 2.6 µm (Figure 17b).[149] Dispersion engineering via changing the diameter of the As_2Se_3 core provided the base for modulation instability occurring in the normal dispersion regime. Far-detuned parametric frequency conversion at 2 µm and 3.5 µm was observed in this fiber structure.

Another example of a hybrid nonlinear fiber is a chalcogenide glass included into a microstructured tellurite fiber by direct fiber drawing an As_2S_3 rod embedded in a structured tellurite perform (**Figure 18**a).[150] The two glasses have almost

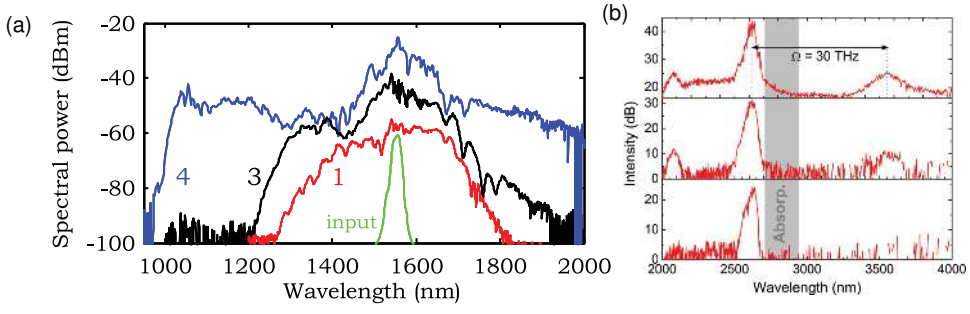

Figure 17. Hybrid chalcogenide–polymer nonlinear fiber waveguides for light generation. a) Octave-spanning supercontinuum generation in a dual layer chalcogenide nanotaper embedded in a polymer matrix. Adapted.[148] Copyright 2014, OSA. b) Mid-IR modulation instability observed in a As_2Se_3/polymer microwire. Adapted with permission.[149] Copyright 2014, OSA.

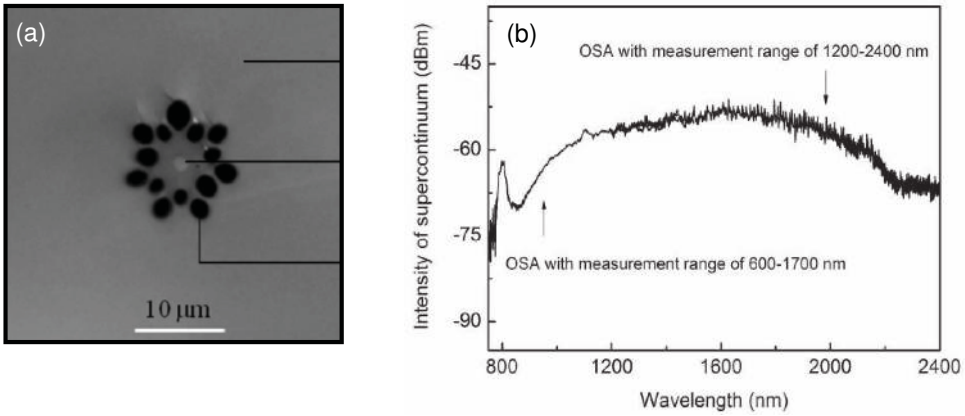

Figure 18. Microstructured hybrid tellurite-chalcogenide fiber fabricated using direct fiber drawing of a chalcogenide-tellurite cane. a) SEM image of a cross section of the fiber. Central circular region is As_2S_3, dark areas are air and the light grey domains correspond to tellurite glass. b) Spectral distribution of the generated supercontinuum in a 1 cm sample when ultrashort pulses were launched into the chalcogenide core. Adapted with permission.[150] Copyright 2009, OSA.

equal thermal expansion coefficients, which is one important prerequisite in thermal drawing as pointed out previously. The dispersion properties of the final hybrid fiber were mainly adjusted via the microstructured cladding and the core diameter (core diameter: 1.5 µm), leading to a flat anomalous group velocity dispersion close to the pump wavelength of 1.85 µm. Very large spanning supercontinuum from about 800 nm to 2.4 µm was generated when ultrashort optical pulses (400 fs) were launched into the central chalcogenide core (Figure 18b).

Due to their good transparency for wavelengths longer than 1 µm and their overall large nonlinearity, silicon core hybrid fibers reveal a substantial potential for being employed for nonlinear light generation in the near and mid-IR. However, compared to the chalcogenide glass systems, one major drawback of silicon is its comparably large two photon cross section when being pump below 2.2 µm.[143] This effect can impose undesired absorption, limiting the maximum achievable spectral bandwidth and density, as observed in planar devices. In recent work, this issue, which had led to silicon-silica fibers being disregarded in nonlinear light generation schemes thus far, was circumvented through the use of hydrogenated amorphous silicon (a-Si:H), integrated into microstructured silica fibers via HPCVD.[151] This material reveals a smaller two-photon absorption parameter due to a larger bandgap energy, and as a result an overall better performance compared to single crystalline silicon. In addition to power-dependent transmission measurements,[152] it was recently shown that new light frequencies can be generated in a 4 mm long a-Si:H silicon–silica hybrid fiber.[153] The relatively small core diameter of 1.7 µm imposes a strong waveguide dispersion on the material dispersion of the silicon, leading to a shift of the zero-dispersion wavelength to about 2 µm. Pumping the system within the anomalous dispersion regime (long-wavelength side of the zero dispersion wavelength), octave-spanning supercontinuum extending from 1.5 µm to 3.1 µm has been generated (**Figure 19**).

Other promising development in fiber-based light generation are optofluidic fibers, in which the strong confinement in a liquid core is used to generate broadband light spectra. To provide total internal reflection at the liquid–solid interface and a sufficiently high optical nonlinearity, low-molecular weight liquids with high refractive index such as carbon-disulfide[154] or carbon tetrachloride[155] are used in selectively filled PCFs or capillaries. One particular interesting feature of liquid core fibers is the emergence of a retarded optical nonlinearity, which is a result of a torque applied to the individual molecules of the liquid when being exposed to strong femtosecond pulses. It was theoretically predicted that this kind of nonlinearity can lead to noninstantaneous solitonic excitations, which does not suffer from a distinct Raman shift towards longer wavelength while propagating through the waveguide.[156] This might pave the way for efficient mid-IR supercontinuum sources on the basis of liquids in fibers.

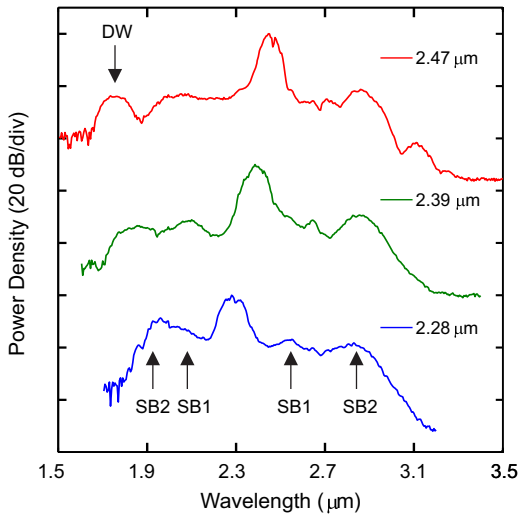

Figure 19. Supercontinuum spectra generated in a dispersion-engineered hydrogenated amorphous silicon-silica hybrid fiber which was fabricated using HPCVD (core diameter: 1.7 µm, sample length 4 mm, zero-dispersion wavelength: 2 µm). The different curves refer to different central pulse wavelength (initial pulse width 300 fs). Adapted with permission.[153] Copyright 2014, OSA.

5.2. Fibers with Sophisticated Functionality

5.2.1. Multifunctional Electro-optic Fibers

Another important class of emerging photonic fiber devices are systems that integrate optical functionalities like waveguiding, reflection or lasing, and allow the modulation of the radiation by a built-in electric field. A first example of this approach relies on the integration of a piezoelectric copolymer (P(VDF)TrFE) inside a flat fiber onto which a Bragg mirror is placed (**Figure 20**a).[75,157] The reflection could be tuned by applying a voltage across the piezoelectric layer. Another advanced fiber device recently developed relied on the modulation of a surface emitting fiber laser by liquid crystal (LC) channels, electrically addressed, where the channels and sandwiching electrodes run along the entire fiber length (Figure 20b).[158,159] When the dye is introduced into the fiber core and pumped with an external laser, lasing can occur through the cavity walls that constitute a Bragg mirror. The polarization of this emitted laser light can be changed as it goes through the LC channel. This modulation is a function of the alignment of LC molecules that is directly related to the potential applied across the electrodes. Note that this fiber device constitutes a good example of a combination of the multimaterial preform-to-fiber fabrication approach and the PAMF method discussed above. Indeed, both he dye and the LC where inserted post-drawing via a pressure assisted melt filling approach inside cavities at prescribed positions. This transverse functionality of direction modulation of an emitted coherent light over large surfaces can pave the way towards a variety of novel devices. The example presented here (Figure 20c) represents an application where such a fiber could be introduced with minimal invasion inside a vessel on which a tumor has grown on one side. Emission could be controlled to illuminate and treat only the tumor and not the surrounding tissue.

5.2.2. Optical Isolation

One of the most important functionalities of photonic devices is to provide direction-dependent propagation loss. This effect, commonly referred to as optical isolation, breaks the time-reversal symmetry of the system and requires the device to be non-reciprocal, which can be achieved either via a traveling wave modulation (e.g., by acousto-optics,[160] by nonlinear optical frequency conversion,[161] or by including a magnetized Faraday medium into the device.[162] The latter is conceptually most relevant from the application point of view since it does not require any sort of external modulation, operates entirely passively, and is input power independent. A Faraday medium requires a diamagnetic or paramagnetic material and a magnetic field applied co-linear to the direction of light propagation. The magnetic field induces a special kind of anisotropy with two off-diagonal elements in the permittivity tensor.[163] The most important material parameter characterizing the magneto-optical (MO) response is the Verdet constant, which is directly proportional to the rotation angle of linearly polarized light.

Many of currently used Faraday materials are single-crystalline and thus are hard to incorporate into optical fibers (e.g., the state-of-the-art material is bismuth-doped yttrium–iron–garnet

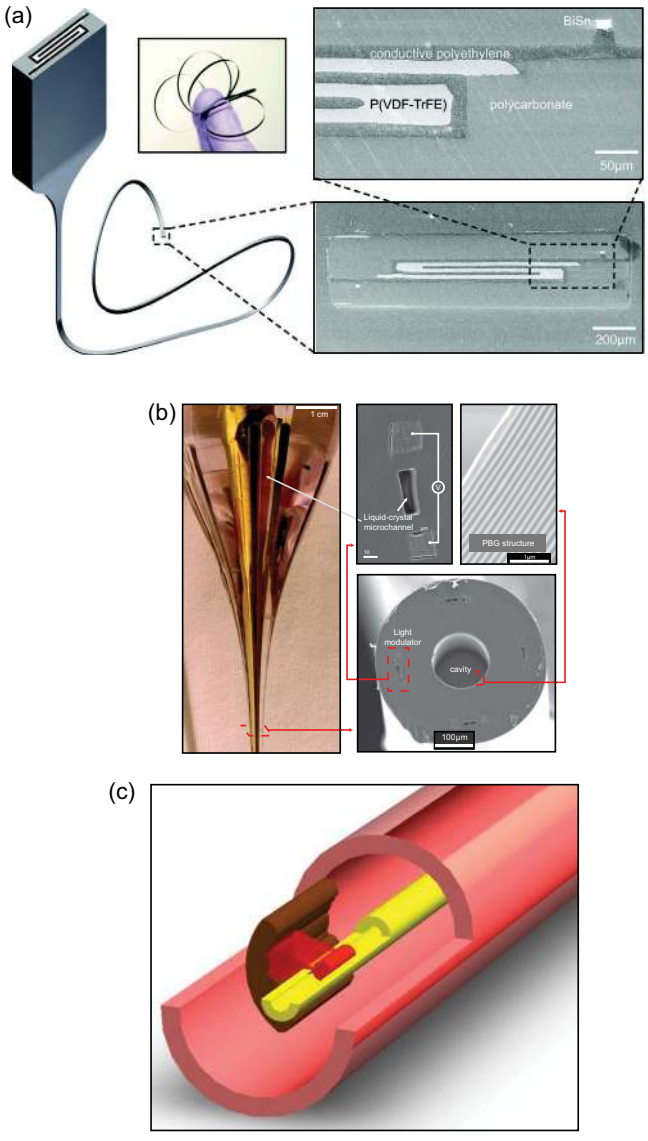

Figure 20. a) A schematic of the drawing process showing the scalability and flexibility of the resulting fiber. The SEM micrograph on the right shows the piezoelectric co-polymer P(VDF)TrFE surrounded by CPE electrode that can modulate the reflection of an incoming beam. Adapted with permission.[157] b) Picture of the preform to fiber neck down region of a hollow core optical fiber integrating hollow channels around the photonic structure. The SEM micrograph shows the fiber cross-section with the Bragg mirror and the electrically addressed channels. c) Schematic of a potential scheme for side emitting fiber laser with direction control that could be used to burn away a tumor growing on one side of the inner part of a vessel. Adapted with permission.[159] Copyright 2012, Macmilllan Publishers Ltd.

(Bi:YIG).[164,165] This issue represents the motivation for investigating diamagnetic or paramagnetic glass systems with large Verdet constants which can be integrated into optical fibers.[166] One of the key questions is how much of the bulk magneto-optic response can be maintained within the fiber and what is the achievable Faraday rotation per absorption length, with the latter being the most important figure-of-merit parameter from the device perspective.[163]

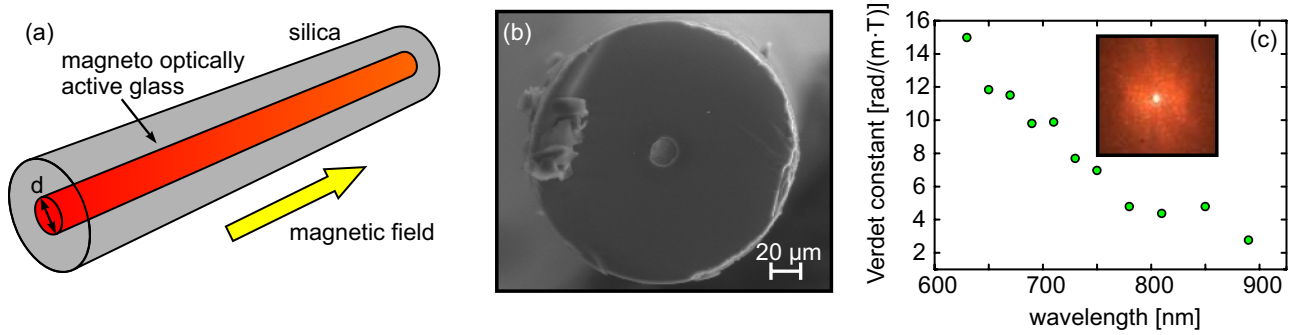

Figure 21. a) Schematic of the magneto-optically active hybrid fiber (red: magneto-optically active core; grey: silica cladding). The yellow arrow indicates the direction of the static magnetic field. b) SEM image of the cross section of the tellurite-silica MO-active fiber (core diameter 20 µm, sample length 8 cm, core glass: $77TeO_2$–$20.5ZnO$-$2.5La_2O_3$). c) Spectral distribution of the effective Verdet constant. The inset shows the guided mode of the fiber when white light is launched into the input. Adapted with permission.[163]

One example of a MO-active HOF has been established by drawing a 65 wt%-terbium-doped silicate perform into fiber, giving rise to a paramagnetic all-fiber Faraday isolator.[167] The effective Verdet constant of that terbium-doped fiber was measured to be 32 rad $(T\ m)^{-1}$, which is 27× larger than that of silica fiber and 83% of the Verdet constant of commercially available crystals used in bulk optics-based isolators. Another example is a MO fiber which has been realized via PAMF and consists of diamagnetic tellurite glass core and a silica cladding (**Figure 21**a,b).[163] The effective Verdet constant defined by the fundamental core mode is about 50% of the bulk value (Figure 21c), indicating morphological variations of the filled glass from the purely isotropic case, which is additionally suggested by the observed magnetic dichroism, which only appears when the glass is filled into fiber. In contrast to the abovementioned silicate fiber, this hybrid fiber has the potential to be fully integrated into current fiber loops as the cladding material is silica.

5.2.3. High Extinction Optical Filtering

The precise selection and filtering of predefined wavelengths from a broad spectrum is essential for many photonic applications, especially in the light of spectral multiplexing. Regarding telecommunication, an ideal filtering element ought to provide a large extinction ratio with an as-steep-as-possible transmission edge over a narrow spectral interval, low intrinsic optical loss and the capability to be spliced directly into fiber circuitry. Here, HOFs and in particular bandgap fibers with high refractive index contrasts represent a promising approach to implement efficient filtering elements.[168–170] One example of a hybrid bandgap fiber with ultrastrong index contrast consists of an array of micrometer-sized chalcogenide strands in a silica matrix with the central strand being omitted (**Figure 22**a,b).[57] The refractive index of the chalcogenide is substantially larger than that of silica, and thus each strand represents a single multimode waveguide. The overlap of evanescent fields hence leads to photonic bandgaps and photonic band windows formation (Figure 22c).[171] Since the dispersion of the band edges are steep with respect to the material dispersion of silica, very strong extinction ratios of more than 60 dB cm^{-1} can be achieved, which is exceptionally high for such an integrated device.

One other example of HOF are PCFs infiltrated with liquids to modify their guidance. Fluid-filled PCFs with a solid core show distinct transmission bands and photonic windows depending on the refractive index contrast between the liquid and solid material and the diameter of the filled bores, assuming the liquid has higher index than the solid.[172] Similarly, hollow-core PCF can be completely filled with liquid that has a lower index than the solid and have the light propagating in a liquid core, with the transmission window shifted relative to the air-filled case by an amount depending on the index of the liquid.[173]

Liquids provide the interesting properties including being sensitive to external influences such as temperature, which makes interesting candidates for the implementation of tunable devices or precise sensing elements.[174] One example includes a MOF with large outer holes and an inner doped silica core, in which the light from the core is coupled to the liquid strand via a long-period grating.[175,176] This device shows a distinct temperature dependence of the resonance peak, which makes it an interesting candidate for environmental sensing. In another example very high refractive-index sensitivity of 30 µm RIU^{-1} (RIU: refractive index unit) have been achieved by selectively filling one hole in the second ring of a PCF with a predefined liquid.[177] An alternative design using a composite fibre made of three different polymers can perform low-index sensing through a single hole in the cladding, which removes the need for selective filling.[178] The index sensitivity is achieved by coupling the core mode to a mode in the adjacent fluid-filled waveguide that is beyond modal cutoff. Examples of sensing in liquid cores include measurements of optical activity in fibres infiltrated with chiral liquids,[173] stimulated Raman spectroscopy of solutions inside a hollow core,[179] and spectral characterization of individual particles suspended in the cores of filled fibres using optical tweezers.[180] Other examples of liquid filled fibers include optofluidic directional mode couplers for viscosity determination[181] and water-core Fresnel fibers.[182]

Semiconductor nanowires introduced in MOFs via PAMF have been used for efficient in-line polarization with a discrimination of more than 10 dB across the entire visible spectrum (**Figure 23**).[58] Using a selective hole closure technique, individual hollow channels in silica PCFs are filled with pure

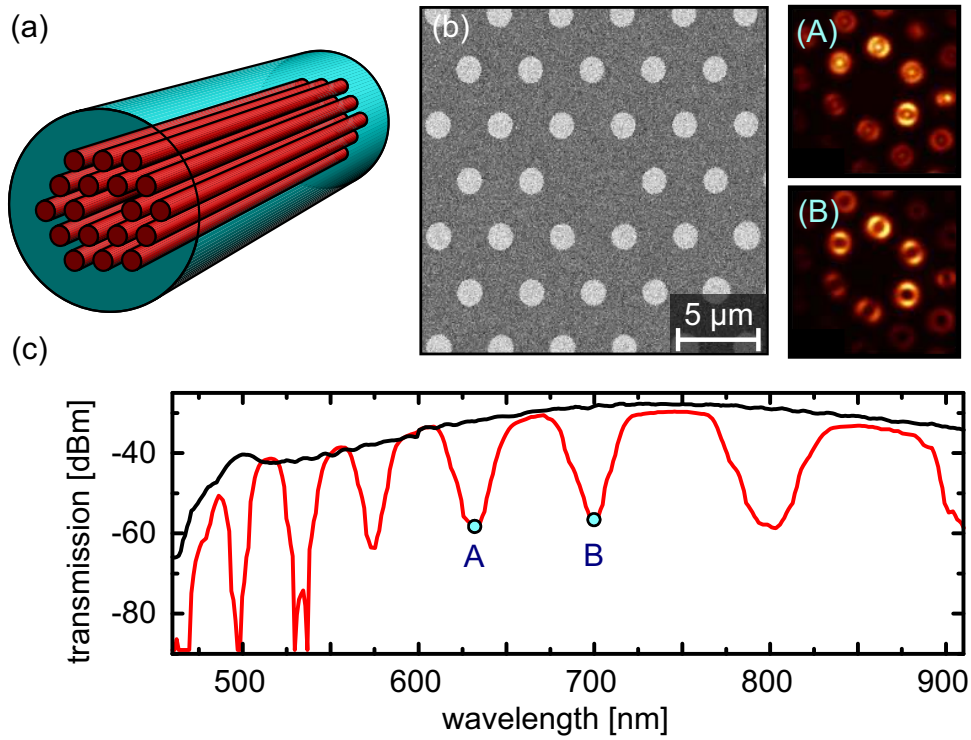

Figure 22. a) Schematic of a photonic bandgap guiding fiber for filtering applications (red: chalcogenide; blue: silica host fiber). b) SEM image of a chalcogenide filled PCF (bright parts: $Ga_4Ge_{21}Sb_{10}S_{65}$ strands, dark grey: silica. Core diameter 7.6 µm, pitch 3.8 µm, strand diameter 1.45 µm). c) Transmission spectrum the bandgap fiber (red) in comparison to an unfilled fiber (black). The point A and B correspond to the output mode patterns shown on the upper right side of the figure (C: 630 nm, D: 700 nm). Adapted with permission.[57] Copyright 2011, OSA.

Germanium. The transmission in the two orthogonal polarization Eigenstates remains spectrally flat with no strong oscillations up to 1 µm and with a polarization discrimination as high as 30 dB in the visible (inset in Figure 23). The strong polarization contrast results from the highly anisotropic modal absorption of the fundamental modes in the fibers, which is an indication of the different modal overlaps with the germanium waveguide. In the IR, strong attenuation peaks are observed, which show a strong temperature dependence of 0.15 nm K^{-1} below 100 °C. These results suggest that the structure forms the basis of a compact optical thermometer. Sensitive temperature determination has also been achieved using polymer infiltrated MOF.[183] This device operates by coupling light from a central glass core to a longitudinal polymer strand via a long-period grating, showing a strong dependence of the spectral position of the resonance dips at ambient temperature.

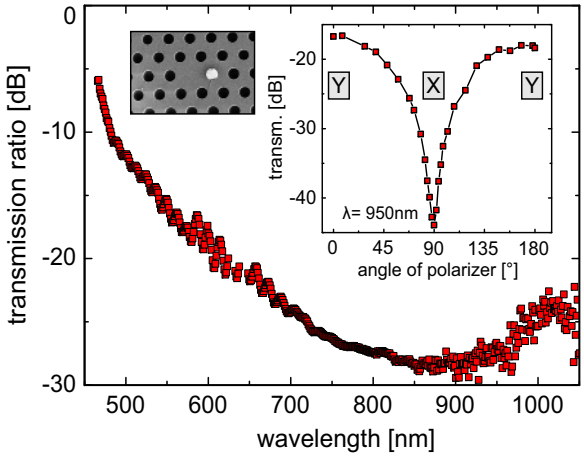

Figure 23. Spectral distribution of the polarization discrimination ratio between the two polarization Eigenstates of the semiconductor inline polarizer. The insets depict the investigated structure, consisting of a Germanium nanowire embedded in a photonic crystal fiber, and the transmission versus analyzer angle at a fixed wavelength (λ_0 = 950 nm). The entire sample length is 1.7 mm. Adapted with permission.[58] Copyright 2008, OSA.

6. Conclusions and Outlook

The overall idea of hybrid optical fibers is to integrate materials, which are traditionally not used in fiber optics, directly into fiber, to impart optical fibers with novel functionalities and expand their field of applications to novel critical areas such as biophotonics, environmental science or quantum optics. Importantly, fibers are no longer viewed as purely axial devices but can also exhibit complex photonic functionalities in their transverse direction. This approach has revitalized fiber optics research with respect to the fiber design itself as well as in rethinking the materials and architectures that can be integrated during drawing or post-processing inside long, thin and flexible one-dimensional fibers. The HOFs discussed in this

review represents a selection of state-of-the-art devices with unique properties, which generally illustrates the potential of this research field from a device and applications perspective. The field has been triggered by improvements in fiber drawing technology and by the emergence of post-processing techniques, accompanied by the investigation of new fiber geometries. From our point of view, we anticipate applications of HOF in the following areas in particular.

6.1. Plasmonics/Metamaterials

As shown in this review, the inclusion of metallic nano- and microwires into fiber has unlocked the areas of plasmonics and metamaterials for fiber optics. Wire array hyperlenses have obvious applications in imaging, as many biologically relevant absorptions (such as vibrations or intermolecular transitions) happen in the mid-IR and THz parts of the spectrum. The use of hyperlenses can deliver very high spatial resolution and new spectral tools to examine important biological samples and processes. New promising applications of fiber-based metamaterials can be envisioned if they are used as novel cladding materials for hollow core fibers, operating non-resonantly in spectral domains which cannot be accessed with current PCF designs. Here, low-loss guidance at mid-IR wavelengths over very board spectral domains or at THz frequencies in subwavelength cores has recently been proposed.[95,96,184] From the plasmonics point of view, the reported nanotips have the potential for establishing a new class of near-field probes if combined with one or more optical waveguides, which can simultaneously deliver and collect light on the nanoscale, leading to new applications in, e.g., molecular disease diagnostics or DNA sequencing. New plasmonic materials can be integrated into fibers, accessing device functionality which cannot be addressed with any of the currently used planar devices. One example are alkali metals, which potentially have excellent plasmonic properties but are exceedingly difficult to handle due to their high chemical reactivity. Moreover, application in sophisticated areas such as superconductivity can be envisioned via including high transition temperature metals into fiber.[72,185]

6.2. Optoelectronics

The direct thermal drawing of multimaterial preforms enables the unique combination of metals, semiconductors and insulators in the cross-section of a uniform, potentially hundreds of kilometer long flexible fiber. This opens novel opportunities for implementing fibers with more complex integrated functionalities such as self-monitoring for non-invasive surgeries,[105] or flexible optical and electronic probing for health care and bio-research.[69] Such multimaterial HOF can also be seen as transverse devices where flexible fibers can interface with their environment in novel ways. Optoelectronic fibers integrating several semiconductor devices can indeed detect light, but also sense local heating, ultrasound waves, or chemicals. Moreover, the combination of photonic crystals with optoelectronic devices is an important thrust of research for photodetectors and photovoltaics.[186–188] Future research directions in the field of optoelectronic fibers will follow this trend by integrating complex architectures to trap and absorb light efficiently. Another direction complements this approach by looking at new materials that can interface with the presented semiconductors, to be used as electrodes or to form rectifying junctions. The integration of junctions represents a unique path to address one bottleneck in current telecommunications networks, namely the interface between optical fibers and planar photonic devices. The designs presented here indicate the enormous potential of HOFs in optoelectronics, and future work will address the issues of electrically connecting the semiconductor junction located within a fiber network.[189,190] A line of work not discussed in this review is the integration of semiconducting nanowires[191] and even microspheres inside thermally drawn fibers.[192,193] With these unconventional fabrications approaches and novel building blocks, innovative ways of trapping light and extracting charges inside optoelectronic fibers can be realized, paving the way towards large area, flexible and even wearable optoelectronic systems with efficiencies on par with current planar and rigid devices.

6.3. Light Generation

The integration of sophisticated dielectric materials provides new degrees of freedom to design fiber devices for light generation with unique properties, being highly relevant in biophotonics and medicine. As shown by the discussed examples, the concept of introducing highly nonlinear materials into fibers allows unique pulse dispersion engineering beyond the capability of all-silica glass fibers, unlocking new applications, for instance, in vibrational spectroscopy or frequency metrology. Further developments will rely on integrating more sophisticated glass and semiconductor systems with predefined properties into fiber, allowing work in spectral domains which are not accessible with all-silica systems, particular in the UV and mid-IR.[194] This includes investigating not only the core glass but also new cladding materials within the scope of PAMF and HPCVD, as for instance tellurite or fluoride glasses can provide promising cladding alternatives when targeting wavelengths longer than 3 μm.[195,196] Moreover materials with improved doping properties can help to implement more efficient fiber lasers, especially for wavelength longer than 3 μm.[197,198] Particularly interesting is the option to use semiconductor junctions for direct in-fiber light generation via direct carrier injection, making external light sources obsolete and thus improving the performance of current telecommunication networks.

Acknowledgements

M. A. Schmidt acknowledges funding from the German Research Foundation (DFG) via the grant number SCHM 2655/3-2. F. Sorin acknowledges funding from the Swiss National Science Foundation via grant number 200021_146871.
The licence on this manuscript was updated and Figure 1 was corrected on January 18, 2016.

Received: June 9, 2015
Revised: August 31, 2015
Published online: October 15, 2015

[1] C. Jauregui, J. Limpert, A. Tunnermann, *Nat. Photonics* **2013**, *7*, 861.
[2] M. E. Fermann, I. Hartl, *Nat. Photonics* **2013**, *7*, 868.
[3] G. P. Agrawal, *Fiber-Optic Communication Systems*, 4th Ed., Wiley, Hoboken, NJ, USA **2010**.
[4] G. P. Agrawal, *J. Opt. Soc. Am. B* **2011**, *28*, A1.
[5] A. Katzir, *Lasers and Optical Fibers in Medicine*, Academic Press, CA, USA, San Diego, **1993**.
[6] V. V. Tuchin, *Proc. SPIE* **1992**, DOI: 10.1117/12.146456.
[7] P. Roriz, O. Frazao, A. B. Lobo-Ribeiro, J. L. Santos, J. A. Simoes, *J. Biomed. Opt.* **2013**, *18*, 50903.
[8] B. Lee, *Opt. Fiber Technol.* **2003**, *9*, 57.
[9] X. W. Ye, Y. H. Su, J. P. Han, *Sci. World J.* **2014**, DOI: 10.1155/2014/652329.
[10] P. S. J. Russell, *J. Lightwave Technol.* **2006**, *24*, 4729.
[11] P. S. J. Russell, *Science* **2003**, *299*, 358.
[12] R. F. Cregan, B. J. Mangan, J. C. Knight, T. A. Birks, P. S. Russell, P. J. Roberts, D. C. Allan, *Science* **1999**, *285*, 1537.
[13] F. Benabid, J. C. Knight, G. Antonopoulos, P. S. J. Russell, *Science* **2002**, *298*, 399.
[14] A. V. V. Nampoothiri, A. M. Jones, C. Fourcade-Dutin, C. C. Mao, N. Dadashzadeh, B. Baumgart, Y. Y. Wang, M. Alharbi, T. Bradley, N. Campbell, F. Benabid, B. R. Washburn, K. L. Corwin, W. Rudolph, *Opt. Mater. Express* **2012**, *2*, 948.
[15] T. A. Birks, J. C. Knight, P. S. Russell, *Opt. Lett.* **1997**, *22*, 961.
[16] A. Hartung, J. Kobelke, A. Schwuchow, J. Bierlich, J. Popp, M. A. Schmidt, T. Frosch, *Opt. Lett.* **2015**, *40*, 3432.
[17] A. Hartung, J. Kobelke, A. Schwuchow, K. Wondraczek, J. Bierlich, J. Popp, T. Frosch, M. A. Schmidt, *Opt. Express* **2014**, *22*, 19131.
[18] F. Yu, J. C. Knight, *Opt. Express* **2013**, *21*, 21466.
[19] F. Poletti, *Opt. Express* **2014**, *22*, 23807.
[20] F. Gerome, R. Jamier, J. L. Auguste, G. Humbert, J. M. Blondy, *Opt. Lett.* **2010**, *35*, 1157.
[21] Z. L. Li, W. Y. Zhou, Y. G. Liu, Q. Ye, Y. Ma, H. F. Wei, J. G. Tian, *Appl. Phys. Lett.* **2013**, *102*, 011136.
[22] P. Zhang, M. Tang, F. Gao, B. P. Zhu, Z. Y. Zhao, L. Duan, S. N. Fu, J. Ouyang, H. F. Wei, P. P. Shum, D. M. Liu, *IEEE Photonics J.* **2015**, *7*, 7100210.
[23] W. Zeng, L. Shu, Q. Li, S. Chen, F. Wang, X. M. Tao, *Adv. Mater.* **2014**, *26*, 5310.
[24] G. M. Tao, A. F. Abouraddy, A. M. Stolyarov, *Int. J. Appl. Glass Sci.* **2012**, *3*, 349.
[25] A. F. Abouraddy, M. Bayindir, G. Benoit, S. D. Hart, K. Kuriki, N. Orf, O. Shapira, F. Sorin, B. Temelkuran, Y. Fink, *Nat. Mater.* **2007**, *6*, 336.
[26] A. Argyros, *J. Lightwave Technol.* **2009**, *27*, 1571.
[27] M. Consales, M. Pisco, A. Cusano, *Photonic Sensors* **2012**, *2*, 289.
[28] G. Kostovski, P. R. Stoddart, A. Mitchell, *Adv. Mater.* **2014**, *26*, 3798.
[29] B. Temelkuran, S. D. Hart, G. Benoit, J. D. Joannopoulos, Y. Fink, *Nature* **2002**, *420*, 650.
[30] S. D. Hart, G. R. Maskaly, B. Temelkuran, P. H. Prideaux, J. D. Joannopoulos, Y. Fink, *Science* **2002**, *296*, 510.
[31] J. C. Knight, *Nature* **2003**, *424*, 847.
[32] G. M. Tao, S. Shabahang, E. H. Banaei, J. J. Kaufman, A. F. Abouraddy, *Opt. Lett.* **2012**, *37*, 2751.
[33] G. M. Tao, S. Shabahang, H. Ren, F. Khalilzadeh-Rezaie, R. E. Peale, Z. Y. Yang, X. S. Wang, A. F. Abouraddy, *Opt. Lett.* **2014**, *39*, 4009.
[34] F. Sorin, A. F. Abouraddy, N. Orf, O. Shapira, J. Viens, J. Arnold, J. D. Joannopoulos, Y. Fink, *Adv. Mater.* **2007**, *19*, 3872.
[35] A. Gumennik, A. M. Stolyarov, B. R. Schell, C. Hou, G. Lestoquoy, F. Sorin, W. McDaniel, A. Rose, J. D. Joannopoulos, Y. Fink, *Adv. Mater.* **2012**, *24*, 6005.
[36] J. D. Joannopoulos, S. G. Johnson, J. N. Winn, R. D. Meade, *Photonic Crystals: Molding the Flow of Light*, Princeton University Press, Princeton, NJ, USA, **2008**.
[37] J. Hou, D. Bird, A. George, S. Maier, B. T. Kuhlmey, J. C. Knight, *Opt. Exp.* **2008**, *16*, 5983.
[38] A. Tuniz, K. J. Kaltenecker, B. M. Fischer, M. Walther, S. C. Fleming, A. Argyros, B. T. Kuhlmey, *Nat. Commun.* **2013**, *4*, 2706.
[39] H. K. Tyagi, H. W. Lee, P. Uebel, M. A. Schmidt, N. Joly, M. Scharrer, P. S. Russell, *Opt. Lett.* **2010**, *35*, 2573.
[40] M. Bayindir, F. Sorin, A. F. Abouraddy, J. Viens, S. D. Hart, J. D. Joannopoulos, Y. Fink, *Nature* **2004**, *431*, 826.
[41] F. Sorin, O. Shapira, A. F. Abouraddy, M. Spencer, N. D. Orf, J. D. Joannopoulos, Y. Fink, *Nano Lett.* **2009**, *9*, 2630.
[42] C. Lu, U. P. Froriep, R. A. Koppes, A. Canales, V. Caggiano, J. Selvidge, E. Bizzi, P. Anikeeva, *Adv. Funct. Mater.* **2014**, *24*, 6594.
[43] J. Ballato, T. Hawkins, P. Foy, R. Stolen, B. Kokuoz, M. Ellison, C. McMillen, J. Reppert, A. M. Rao, M. Daw, S. Sharma, R. Shori, O. Stafsudd, R. R. Rice, D. R. Powers, *Opt. Express* **2008**, *16*, 18675.
[44] G. W. Tang, Q. Qian, X. Wen, G. X. Zhou, X. D. Chen, M. Sun, D. D. Chen, Z. M. Yang, *J. Alloy Compd.* **2015**, *633*, 1.
[45] A. Tuniz, R. Lwin, A. Argyros, S. C. Fleming, E. M. Pogson, E. Constable, R. A. Lewis, B. T. Kuhlmey, *Opt. Express* **2011**, *19*, 16480.
[46] H. W. Lee, M. A. Schmidt, R. F. Russell, N. Y. Joly, H. K. Tyagi, P. Uebel, P. S. J. Russell, *Opt. Express* **2011**, *19*, 12180.
[47] N. Da, A. A. Enany, N. Granzow, M. A. Schmidt, P. S. Russell, L. Wondraczek, *J. Non-Cryst. Solids* **2011**, *357*, 1558.
[48] N. Da, L. Wondraczek, M. A. Schmidt, N. Granzow, P. S. J. Russell, *J. Non-Cryst. Solids* **2010**, *356*, 1829.
[49] R. H. Doremus, *J. Appl. Phys.* **2002**, *92*, 7619.
[50] M. A. Schmidt, L. N. Prill Sempere, H. K. Tyagi, C. G. Poulton, P. S. J. Russell, *Phys. Rev. B* **2008**, *77*, 033417.
[51] E. W. Washburn, *Phys. Rev.* **1921**, *17*, 273.
[52] M. A. Schmidt, P. S. J. Russell, *Opt. Express* **2008**, *16*, 13617.
[53] H. W. Lee, M. A. Schmidt, P. S. J. Russell, *Opt. Lett.* **2012**, *37*, 2946.
[54] P. Uebel, M. A. Schmidt, H. W. Lee, P. S. J. Russell, *Opt. Express* **2012**, *20*, 28409.
[55] N. Granzow, M. A. Schmidt, W. Chang, L. Wang, Q. Coulombier, J. Troles, P. Toupin, I. Hartl, K. F. Lee, M. E. Fermann, L. Wondraczek, P. S. J. Russell, *Opt. Express* **2013**, *21*, 10969.
[56] K. F. Lee, N. Granzow, M. A. Schmidt, W. Chang, L. Wang, Q. Coulombier, J. Troles, N. Leindecker, K. L. Vodopyanov, P. G. Schunemann, M. E. Fermann, P. S. J. Russell, I. Hartl, *Opt. Lett.* **2014**, *39*, 2056.
[57] N. Granzow, P. Uebel, M. A. Schmidt, A. S. Tverjanovich, L. Wondraczek, P. S. Russell, *Opt. Lett.* **2011**, *36*, 2432.
[58] H. K. Tyagi, M. A. Schmidt, L. P. Sempere, P. S. J. Russell, *Opt. Express* **2008**, *16*, 17227.
[59] N. Granzow, S. P. Stark, M. A. Schmidt, A. S. Tverjanovich, L. Wondraczek, P. S. J. Russell, *Opt. Express* **2011**, *19*, 21003.
[60] P. J. A. Sazio, A. Amezcua-Correa, C. E. Finlayson, J. R. Hayes, T. J. Scheidemantel, N. F. Baril, B. R. Jackson, D. J. Won, F. Zhang, E. R. Margine, V. Gopalan, V. H. Crespi, J. V. Badding, *Science* **2006**, *311*, 1583.
[61] B. R. Jackson, P. J. A. Sazio, J. V. Badding, *Adv. Mater.* **2008**, *20*, 1135.
[62] N. Healy, S. Mailis, N. M. Bulgakova, P. J. A. Sazio, T. D. Day, J. R. Sparks, H. Y. Cheng, J. V. Badding, A. C. Peacock, *Nat. Mater.* **2014**, *13*, 1122.
[63] D. J. Won, M. O. Ramirez, H. Kang, V. Gopalan, N. F. Baril, J. Calkins, J. V. Badding, P. J. A. Sazio, *Appl. Phys. Lett.* **2007**, *91*, 161112.
[64] C. E. Finlayson, A. Amezcua-Correa, P. J. A. Sazio, N. F. Baril, J. V. Badding, *Appl. Phys. Lett.* **2007**, *90*, 132110.
[65] R. R. He, P. J. A. Sazio, A. C. Peacock, N. Healy, J. R. Sparks, M. Krishnamurthi, V. Gopalan, J. V. Badding, *Nat. Photonics* **2012**, *6*, 174.
[66] P. Mehta, M. Krishnamurthi, N. Healy, N. F. Baril, J. R. Sparks, P. J. A. Sazio, V. Gopalan, J. V. Badding, A. C. Peacock, *Appl. Phys. Lett.* **2010**, *97*, 071117.

[67] J. R. Sparks, R. R. He, N. Healy, S. Chaudhuri, T. C. Fitzgibbons, A. C. Peacock, P. J. A. Sazio, J. V. Badding, *Adv. Funct. Mater.* **2013**, *23*, 1647.
[68] F. Zhang, A. M. Aravanis, A. Adamantidis, L. de Lecea, K. Deisseroth, *Nat. Rev. Neurosci.* **2007**, *8*, 577.
[69] A. Canales, X. T. Jia, U. P. Froriep, R. A. Koppes, C. M. Tringides, J. Selvidge, C. Lu, C. Hou, L. Wei, Y. Fink, P. Anikeeva, *Nat. Biotechnol.* **2015**, *33*, 277.
[70] H. Knape, W. Margulis, *Opt. Lett.* **2007**, *32*, 614.
[71] D. Lopez-Cortes, O. Tarasenko, W. Margulis, *Opt. Lett.* **2012**, *37*, 3288.
[72] D. Homa, Y. Liang, G. Pickrell, *Appl. Phys. Lett.* **2013**, *103*, 082601.
[73] D. Homa, Y. X. Liang, C. Hill, G. Kaur, G. Pickrell, *Appl. Phys. A–Mater* **2015**, *118*, 23.
[74] W. Margulis, *Laser Focus World* **2008**, *44*, 15.
[75] S. Egusa, Z. Wang, N. Chocat, Z. M. Ruff, A. M. Stolyarov, D. Shemuly, F. Sorin, P. T. Rakich, J. D. Joannopoulos, Y. Fink, *Nat. Mater.* **2010**, *9*, 643.
[76] F. Sorin, G. Lestoquoy, S. Danto, J. D. Joannopoulos, Y. Fink, *Opt. Express* **2010**, *18*, 24264.
[77] J. A. F. Gu, S. Gorgutsa, M. Skorobogatiy, *Appl. Phys. Lett.* **2010**, *97*, 133305.
[78] M. Rioux, Y. Ledemi, J. Viens, S. Morency, S. A. Ghaffari, Y. Messaddeq, *RSC Adv.* **2015**, *5*, 40236.
[79] R. Spittel, P. Uebel, H. Bartelt, M. A. Schmidt, *Opt. Express* **2015**, *23*, 12174.
[80] P. Uebel, M. A. Schmidt, S. T. Bauerschmidt, P. S. J. Russell, *Appl. Phys. Lett.* **2013**, *103*, 021101.
[81] S. W. Hell, J. Wichmann, *Opt. Lett.* **1994**, *19*, 780.
[82] R. Dorn, S. Quabis, G. Leuchs, *Phys. Rev. Lett.* **2003**, *91*, 233901.
[83] P. Uebel, M. A. Schmidt, M. Scharrer, P. S. Russell, *New J. Phys.* **2011**, *13*, 63016.
[84] J. D. Jackson, *Classical Electrodynamics*, Wiley, New York, **1975**.
[85] J. B. Pendry, A. J. Holden, W. J. Stewart, I. Youngs, *Phys. Rev. Lett.* **1996**, *76*, 4773.
[86] R. C. McPhedran, I. V. Shadrivov, B. T. Kuhlmey, Y. S. Kivshar, *NPG Asia Mater.* **2011**, *3*, 100.
[87] J. B. Pendry, A. J. Holden, D. J. Robbins, W. J. Stewart, *IEEE T. Microw. Theory* **1999**, *47*, 2075.
[88] C. R. Simovski, P. A. Belov, A. V. Atrashchenko, Y. S. Kivshar, *Adv. Mater.* **2012**, *24*, 4229.
[89] A. Argyros, A. Tuniz, S. C. Fleming, B. T. Kuhlmey, *Drawn Metamaterials*, Elsevier, Great Britain **2015**.
[90] A. Tuniz, R. Lwin, A. Argyros, S. C. Fleming, B. T. Kuhlmey, *Jove-J. Vis. Exp.* **2012**, *68*, e4299.
[91] A. Tuniz, B. T. Kuhlmey, R. Lwin, A. Wang, J. Anthony, R. Leonhardt, S. C. Fleming, *Appl. Phys. Lett.* **2010**, *96*, 191101.
[92] O. T. Naman, M. R. New-Tolley, R. Lwin, A. Tuniz, A. H. Al-Janabi, I. Karatchevtseva, S. C. Fleming, B. T. Kuhlmey, A. Argyros, *Adv. Opt. Mater.* **2013**, *1*, 971.
[93] X. D. Yang, J. Yao, J. Rho, X. B. Yin, X. Zhang, *Nat. Photonics* **2012**, *6*, 450.
[94] N. Singh, A. Tuniz, R. Lwin, S. Atakaramians, A. Argyros, S. C. Fleming, B. T. Kuhlmey, *Opt. Mater. Express* **2012**, *2*, 1254.
[95] S. Atakaramians, A. Argyros, S. C. Fleming, B. T. Kuhlmey, *J. Opt. Soc. Am. B* **2013**, *30*, 851.
[96] M. Yan, N. A. Mortensen, *Opt. Express* **2009**, *17*, 14851.
[97] A. Tuniz, D. Ireland, L. Poladian, A. Argyros, C. M. de Sterke, B. T. Kuhlmey, *Opt. Lett.* **2014**, *39*, 3286.
[98] P. A. Belov, C. R. Simovski, P. Ikonen, *Phys. Rev. B* **2005**, *71*, 193105.
[99] M. G. Silveirinha, P. A. Belov, C. R. Simovski, *Opt. Lett.* **2008**, *33*, 1726.
[100] J. Hou, D. Bird, A. George, S. A. Maier, B. T. Kuhlmey, J. C. Knight, *Opt. Express* **2008**, *16*, 5983.
[101] E. J. Smith, Z. W. Liu, Y. F. Mei, O. G. Schmidt, *Nano Lett.* **2010**, *10*, 1.
[102] R. Spittel, H. Bartelt, M. A. Schmidt, *Opt. Express* **2014**, *22*, 11741.
[103] A. F. Abouraddy, O. Shapira, M. Bayindir, J. Arnold, F. Sorin, D. S. Hinczewski, J. D. Joannopoulos, Y. Fink, *Nat. Mater.* **2006**, *5*, 532.
[104] F. Sorin, O. Shapira, A. F. Abouraddy, Y. Fink, *SPIE Newsroom* **2009**, DOI:10.1117/2.1200911.1760.
[105] M. Bayindir, O. Shapira, D. Saygin-Hinczewski, J. Viens, A. F. Abouraddy, J. D. Joannopoulos, Y. Fink, *Nat. Mater.* **2005**, *4*, 820.
[106] N. D. Orf, O. Shapira, F. Sorin, S. Danto, M. A. Baldo, J. D. Joannopoulos, Y. Fink, *Proc. Natl. Acad. Sci. USA* **2011**, *108*, 4743.
[107] M. Bayindir, A. E. Abouraddy, J. Arnold, J. D. Joannopoulos, Y. Fink, *Adv. Mater.* **2006**, *18*, 845.
[108] B. J. Eggleton, B. Luther-Davies, K. Richardson, *Nat Photonics* **2011**, *5*, 141.
[109] A. Zakery, S. R. Elliott, *Optical Nonlinearities in Chalcogenide Glasses and their Applications*, Springer, Berlin, Berlin, Germany, **2007**.
[110] J. Troles, L. Brilland, F. Smektala, P. Houizot, F. Desevedavy, Q. Coulombier, N. Traynor, T. Chartier, T. N. Nguyen, J. L. Adam, G. Renversez, *Fiber Integrated Opt.* **2009**, *28*, 11.
[111] B. Gates, B. Mayers, B. Cattle, Y. N. Xia, *Adv. Funct. Mater.* **2002**, *12*, 219.
[112] G. G. Roberts, *J. Phys. C Solid* **1971**, *4*, 1348.
[113] H. T. Li, P. J. Regensburger, *J. Appl. Phys.* **1963**, *34*, 1730.
[114] M. D. Tabak, *Appl. Opt.* **1969**, *8*, 4.
[115] T. Unold, H. W. Schock, *Annu. Rev. Mater. Res.* **2011**, *41*, 297.
[116] R. Lechner, S. Jost, J. Palm, M. Gowtham, F. Sorin, B. Louis, H. Yoo, R. A. Wibowo, R. Hock, *Thin Solid Films* **2013**, *535*, 5.
[117] H. Yoo, R. A. Wibowo, A. Holzing, R. Lechner, J. Palm, S. Jost, M. Gowtham, F. Sorin, B. Louis, R. Hock, *Thin Solid Films* **2013**, *535*, 73.
[118] L. I. Berger, *Semiconductor Materials*, CRC Press, Boca Radon, FL, USA, **1996**.
[119] S. Danto, F. Sorin, N. D. Orf, Z. Wang, S. A. Speakman, J. D. Joannopoulos, Y. Fink, *Adv. Mater.* **2010**, *22*, 4162.
[120] S. Danto, Z. Ruff, Z. Wang, J. D. Joannopoulos, Y. Fink, *Adv. Funct. Mater.* **2011**, *21*, 1095.
[121] A. M. Stolyarov, A. Gumennik, W. McDaniel, O. Shapira, B. Schell, F. Sorin, K. Kuriki, G. Benoit, A. Rose, J. D. Joannopoulos, Y. Fink, *Opt. Express* **2012**, *20*, 12407.
[122] V. Raghunathan, D. Borlaug, R. R. Rice, B. Jalali, *Opt. Express* **2007**, *15*, 14355.
[123] N. K. Hon, R. Soref, B. Jalali, *J. Appl. Phys.* **2011**, *110*, 11301.
[124] B. Scott, K. Wang, V. Caluori, G. Pickrell, *Opt. Eng.* **2009**, *48*, 100501.
[125] J. Ballato, T. Hawkins, P. Foy, B. Yazgan-Kokuoz, R. Stolen, C. McMillen, N. K. Hon, B. Jalali, R. Rice, *Opt. Express* **2009**, *17*, 8029.
[126] J. Ballato, T. Hawkins, P. Foy, C. McMillen, L. Burka, J. Reppert, R. Podila, A. M. Rao, R. R. Rice, *Opt. Express* **2010**, *18*, 4972.
[127] P. Dragic, T. Hawkins, P. Foy, S. Morris, J. Ballato, *Nat. Photonics* **2012**, *6*, 627.
[128] C. Hou, X. T. Jia, L. Wei, S. C. Tan, X. Zhao, J. D. Joannopoulos, Y. Fink, *Nat. Commun.* **2015**, *6*, 6248.
[129] C. McMillen, G. Brambilla, S. Morris, T. Hawkins, P. Foy, N. Broderick, E. Koukharenko, R. Rice, J. Ballato, *Opt. Mater.* **2012**, *35*, 93.
[130] N. Gupta, C. McMillen, R. Singh, R. Podila, A. M. Rao, T. Hawkins, P. Foy, S. Morris, R. Rice, K. F. Poole, L. Zhu, J. Ballato, *J. Appl. Phys.* **2011**, *110*, 093107.
[131] S. Morris, C. McMillen, T. Hawkins, P. Foy, R. Stolen, J. Ballato, R. Rice, *J. Cryst. Growth* **2012**, *352*, 53.
[132] G. W. Tang, Q. Qian, K. L. Peng, X. Wen, G. X. Zhou, M. Sun, X. D. Chen, Z. M. Yang, *AIP Adv.* **2015**, *5*, 027113.

[133] C. Hou, X. T. Jia, L. Wei, A. M. Stolyarov, O. Shapira, J. D. Joannopoulos, Y. Fink, *Nano Lett.* **2013**, *13*, 975.
[134] E. Snitzer, R. Tumminelli, *Opt. Lett.* **1989**, *14*, 757.
[135] B. O'Connor, K. P. Pipe, M. Shtein, *Appl. Phys. Lett.* **2008**, *92*, 193306.
[136] R. R. He, T. D. Day, M. Krishnamurthi, J. R. Sparks, P. J. A. Sazio, V. Gopalan, J. V. Badding, *Adv. Mater.* **2013**, *25*, 1461.
[137] E. H. Banaei, A. F. Abouraddy, *Prog. Photovoltaics* **2015**, *23*, 403.
[138] J. M. Dudley, G. Genty, S. Coen, *Rev. Mod. Phys.* **2006**, *78*, 1135.
[139] J. Herrmann, U. Griebner, N. Zhavoronkov, A. Husakou, D. Nickel, J. C. Knight, W. J. Wadsworth, P. S. J. Russell, G. Korn, *Phys. Rev. Lett.* **2002**, *88*, 173901.
[140] D. I. Yeom, E. C. Maegi, M. R. E. Lamont, M. A. F. Roelens, L. B. Fu, B. J. Eggleton, *Opt. Lett.* **2008**, *33*, 660.
[141] D. D. Hudson, S. A. Dekker, E. C. Maegi, A. C. Judge, S. D. Jackson, E. B. Li, J. S. Sanghera, L. B. Shaw, I. D. Aggarwal, B. J. Eggleton, *Opt. Lett.* **2011**, *36*, 1122.
[142] D. D. Hudson, M. Baudisch, D. Werdehausen, B. J. Eggleton, J. Biegert, *Opt. Lett.* **2014**, *39*, 5752.
[143] R. K. W. Lau, M. R. E. Lamont, A. G. Griffith, Y. Okawachi, M. Lipson, A. L. Gaeta, *Opt. Lett.* **2014**, *39*, 4518.
[144] M. A. Foster, A. L. Gaeta, *Opt. Express* **2004**, *12*, 3137.
[145] S. R. Xie, F. Tani, J. C. Travers, P. Uebel, C. Caillaud, J. Troles, M. A. Schmidt, P. S. J. Russell, *Opt. Lett.* **2014**, *39*, 5216.
[146] A. Zakery, S. R. Elliott, *Optical Nonlinearities in Chalcogenide Glasses and their Applications*, Spinger, Berlin **2007**.
[147] S. Wang, C. Jain, L. Wondraczek, K. Wondraczek, J. Kobelke, J. Troles, C. Caillaud, M. A. Schmidt, *Appl. Phys. Lett.* **2015**, *106*, 201908.
[148] S. Shabahang, G. M. Tao, M. P. Marquez, H. H. Hu, T. R. Ensley, P. J. Delfyett, A. F. Abouraddy, *J. Opt. Soc. Am. B* **2014**, *31*, 450.
[149] T. Godin, Y. Combes, R. Ahmad, M. Rochette, T. Sylvestre, J. M. Dudley, *Opt. Lett.* **2014**, *39*, 1885.
[150] M. S. Liao, C. Chaudhari, G. S. Qin, X. Yan, C. Kito, T. Suzuki, Y. Ohishi, M. Matsumoto, T. Misumi, *Opt. Express* **2009**, *17*, 21608.
[151] N. F. Baril, R. R. He, T. D. Day, J. R. Sparks, B. Keshavarzi, M. Krishnamurthi, A. Borhan, V. Gopalan, A. C. Peacock, N. Healy, P. J. A. Sazio, J. V. Badding, *J. Am. Chem. Soc.* **2012**, *134*, 19.
[152] L. Shen, N. Healy, P. Mehta, T. D. Day, J. R. Sparks, J. V. Badding, A. C. Peacock, *Opt. Express* **2013**, *21*, 13075.
[153] L. Shen, N. Healy, L. Xu, H. Y. Cheng, T. D. Day, J. H. V. Price, J. V. Badding, A. C. Peacock, *Opt. Lett.* **2014**, *39*, 5721.
[154] S. Kedenburg, T. Gissibl, T. Steinle, A. Steinmann, H. Giessen, *Opt. Express* **2015**, *23*, 8281.
[155] M. Vieweg, T. Gissibl, S. Pricking, B. T. Kuhlmey, D. C. Wu, B. J. Eggleton, H. Giessen, *Opt. Express* **2010**, *18*, 25232.
[156] C. Conti, M. A. Schmidt, P. S. J. Russell, F. Biancalana, *Phys. Rev. Lett.* **2010**, *105*, 263902.
[157] N. Chocat, G. Lestoquoy, Z. Wang, D. M. Rodgers, J. D. Joannopoulos, Y. Fink, *Adv. Mater.* **2012**, *24*, 5327.
[158] A. M. Stolyarov, L. Wei, F. Sorin, G. Lestoquoy, J. D. Joannopoulos, Y. Fink, *Appl. Phys. Lett.* **2012**, *101*, 011108.
[159] A. M. Stolyarov, L. Wei, O. Shapira, F. Sorin, S. L. Chua, J. D. Joannopoulos, Y. Fink, *Nat. Photonics* **2012**, *6*, 229.
[160] M. S. Kang, A. Butsch, P. S. Russell, *Nat. Photonics* **2011**, *5*, 549.
[161] Z. F. Yu, S. H. Fan, *Nat. Photonics* **2009**, *3*, 91.
[162] J. P. Krumme, V. Doormann, C. P. Klages, *Appl. Opt.* **1984**, *23*, 1184.
[163] M. A. Schmidt, L. Wondraczek, H. W. Lee, N. Granzow, N. Da, P. S. Russell, *Adv. Mater.* **2011**, *23*, 2681.
[164] V. Doormann, J. P. Krumme, H. Lenz, *J. Appl. Phys.* **1990**, *68*, 3544.
[165] G. F. Dionne, G. A. Allen, *J. Appl. Phys.* **1993**, *73*, 6127.
[166] A. Winterstein, H. Akamatsu, D. Moncke, K. Tanaka, M. A. Schmidt, L. Wondraczek, *Opt. Mater. Express* **2013**, *3*, 184.
[167] L. Sun, S. Jiang, J. R. Marciante, *Opt. Express* **2010**, *18*, 12191.
[168] M. A. Schmidt, N. Granzow, N. Da, M. Peng, L. Wondraczek, P. S. J. Russell, *Opt. Lett.* **2009**, *34*, 1946.
[169] F. Luan, A. K. George, T. D. Hedley, G. J. Pearce, D. M. Bird, J. C. Knight, P. S. J. Russell, *Opt. Lett.* **2004**, *29*, 2369.
[170] A. Argyros, T. A. Birks, S. G. Leon-Saval, C. M. B. Cordeiro, F. Luan, P. S. J. Russell, *Opt. Express* **2005**, *13*, 309.
[171] T. A. Birks, G. J. Pearce, D. M. Bird, *Opt. Express* **2006**, *14*, 9483.
[172] B. T. Kuhlmey, B. J. Eggleton, D. K. C. Wu, *J. Lightwave Technol.* **2009**, *27*, 1617.
[173] F. M. Cox, A. Argyros, M. C. J. Large, *Opt. Express* **2006**, *14*, 4135.
[174] C. Monat, P. Domachuk, B. J. Eggleton, *Nat. Photonics* **2007**, *1*, 106.
[175] P. Mach, M. Dolinski, K. W. Baldwin, J. A. Rogers, C. Kerbage, R. S. Windeler, B. J. Eggleton, *Appl. Phys. Lett.* **2002**, *80*, 4294.
[176] C. Kerbage, B. J. Eggleton, *Opt. Fiber Technol.* **2004**, *10*, 133.
[177] D. K. C. Wu, B. T. Kuhlmey, B. J. Eggleton, *Opt. Lett.* **2009**, *34*, 322.
[178] K. J. Lee, X. Q. Liu, N. Vuillemin, R. Lwin, S. G. Leon-Saval, A. Argyros, B. T. Kuhlmey, *Opt. Express* **2014**, *22*, 17497.
[179] F. M. Cox, A. Argyros, M. C. J. Large, S. Kalluri, *Opt. Express* **2007**, *15*, 13675.
[180] C. Rajapakse, F. Wang, T. C. Y. Tang, P. J. Reece, S. G. Leon-Saval, A. Argyros, *Opt. Express* **2012**, *20*, 11232.
[181] H. W. Lee, M. A. Schmidt, P. Uebel, H. Tyagi, N. Y. Joly, M. Scharrer, P. S. Russell, *Opt. Express* **2011**, *19*, 8200.
[182] C. Martelli, J. Canning, K. Lyytikainen, N. Groothoff, *Opt. Express* **2005**, *13*, 3890.
[183] B. J. Eggleton, C. Kerbage, P. S. Westbrook, R. S. Windeler, A. Hale, *Opt. Express* **2001**, *9*, 698.
[184] S. Atakaramians, A. Argyros, S. C. Fleming, B. T. Kuhlmey, *J. Opt. Soc. Am. B* **2012**, *29*, 2462.
[185] D. Homa, Y. X. Liang, G. Pickrell, *J. Supercond. Nov. Magn.* **2014**, *27*, 891.
[186] P. Bermel, C. Luo, L. Zeng, L. C. Kimerling, J. D. Joannopoulos, *Opt. Express* **2007**, *15*, 16986.
[187] B. Brudieu, A. Le Bris, J. Teisseire, F. Guillemot, G. Dantelle, S. Misra, P. R. I. Cabarrocas, F. Sorin, T. Gacoin, *Adv. Opt. Mater.* **2014**, *2*, 1105.
[188] K. X. Z. Wang, Z. F. Yu, V. Liu, A. Raman, Y. Cui, S. H. Fan, *Energ. Environ. Sci.* **2014**, *7*, 2725.
[189] G. Chesini, C. M. B. Cordeiro, C. J. S. de Matos, M. Fokine, I. C. S. Carvalho, J. C. Knight, *Opt. Express* **2009**, *17*, 1660.
[190] A. van Brakel, C. Grivas, M. N. Petrovich, D. J. Richardson, *Opt. Express* **2007**, *15*, 8731.
[191] D. S. Deng, N. D. Orf, A. F. Abouraddy, A. M. Stolyarov, J. D. Joannopoulos, H. A. Stone, Y. Fink, *Nano Lett.* **2008**, *8*, 4265.
[192] A. Gumennik, L. Wei, G. Lestoquoy, A. M. Stolyarov, X. T. Jia, P. H. Rekemeyer, M. J. Smith, X. D. Liang, B. J. B. Grena, S. G. Johnson, S. Gradecak, A. F. Abouraddy, J. D. Joannopoulos, Y. Fink, *Nat. Commun.* **2013**, *4*, 2216.
[193] J. J. Kaufman, G. M. Tao, S. Shabahang, E. H. Banaei, D. S. S. Deng, X. D. Liang, S. G. Johnson, Y. Fink, A. F. Abouraddy, *Nature* **2012**, *487*, 463.
[194] X. Jiang, N. Y. Joly, M. A. Finger, F. Babic, G. K. L. Wong, J. C. Travers, P. S. Russell, *Nat. Photonics* **2015**, *9*, 133.
[195] S. Manning, H. Ebendorff-Heidepriem, T. M. Monro, *Opt. Mater. Express* **2012**, *2*, 140.
[196] T. M. Monro, H. Ebendorff-Heidepriem, *Annu. Rev. Mater. Res.* **2006**, *36*, 467.
[197] A. Stronski, O. Paiuk, A. Gudymenko, V. Klad'ko, P. Oleksenko, N. Vuichyk, M. Vlcek, I. Lishchynskyy, E. Lahderanta, A. Lashkul, A. Gubanova, T. Krys'kov, *Ceram. Int.* **2015**, *41*, 7543.
[198] Y. J. He, X. S. Wang, Q. H. Nie, Y. S. Xu, G. X. Wang, T. F. Xu, S. X. Dai, *Infrared Phys. Techn.* **2013**, *58*, 1.